

This manuscript has been submitted for publication in **JOURNAL OF CONTAMINANT HYDROLOGY**. Please note that, despite having undergone peer review, the manuscript has yet to be formally accepted for publication. Subsequent versions of this manuscript may have slightly different content. If accepted, the final version of this manuscript will be available via the '***Peer-reviewed Publication DOI***' link on the right-hand side of this webpage. Please feel free to contact any of the authors; we welcome feedback.

Journal of Contaminant Hydrology

Quantifying salinity in heterogeneous coastal aquifers through ERT and IP: insights from laboratory and field investigations

--Manuscript Draft--

Manuscript Number:	
Article Type:	Research Paper
Keywords:	aquifer, saltwater intrusion, conductivity, resistivity, induced polarization.
Corresponding Author:	Diep Cong-Thi, Ph.D student BELGIUM
First Author:	Diep Cong-Thi, Ph.D student
Order of Authors:	Diep Cong-Thi, Ph.D student Linh Pham Dieu David Caterina Xavier De Pauw Huyen Dang Thi Hieu Huu Ho Frédéric Nguyen Thomas Hermans
Abstract:	<p>The lithological and stratigraphical heterogeneity of coastal aquifers has a great influence on saltwater intrusion (SI). This makes it difficult to predict SI pathways and their persistence in time. In this context, electrical resistivity tomography (ERT) and induced polarization (IP) methods are receiving increasing attention regarding the discrimination between saltwater-bearing and clayey sediments. To simplify the interpretation of ERT data, it is commonly assumed that the bulk conductivity mostly depends on the conductivity of pore-filling fluids, while surface conductivity is generally disregarded in the spatial and temporal variability of the aquifers, particularly, once the aquifer is affected by the presence of saltwater. Quantifying salinities based on a simplified petrophysical relationship can lead to misinterpretation in aquifers constituted by clay-rich sediments. In this study, we rely on co-located data from drilled boreholes to formulate petrophysical relationships between bulk and fluid conductivity for clay-bearing and clay-free sediments. First, the sedimentary samples from the drilled wells were classified according to their particle size distribution and analyzed in the lab using a SIP in controlled salinity conditions to derive their formation factors, surface conductivity and chargeability. Second, the deduced thresholds are applied on the field to distinguish clay-bearing sediments from brackish sandy sediments. The results are validated with logging data and direct salinity measurements on water samples. We applied the approach along the Luy River Catchment and find that the formation factors and surface conductivity of the different unconsolidated sedimentary classifications are varying from 4.0 to 8.9 for coarse-grained sand and clay-bearing mixtures, while normalized chargeability above 1.5 mS/m indicates the presence of clay. The clay-bearing sediments are mostly distributed in discontinuous small lenses. The assumption of homogenous geological media is therefore leading to overestimating SI in the heterogeneous clay-bearing aquifers.</p>
Suggested Reviewers:	Damien Jougnot damien.jougnot@upmc.fr An expert in petrophysical relationships related to clay responses and saltwater intrusion. Lee Slater lslater@newark.rutgers.edu An expert in hydrogeophysics, particularly in saline-contamination Adrian Flores Orozco

adrian.flores-oroeco@geo.tuwien.ac.at
An expert in geophysics.

1 Quantifying salinity in heterogeneous coastal aquifers 2 through ERT and IP: insights from laboratory and field 3 investigations

4 D. Cong-Thi^{1,2}, L. Pham Dieu^{1,2}, D. Caterina³, X. De Pauw¹, H. Dang Thi², HH. Ho², F. Nguyen^{3,4},
5 T. Hermans¹

6 (1) Department of Geology, Ghent University, 9000-Gent, Belgium.

7 (2) Department of Marine Geology, Vietnam Institute of Geosciences and Mineral Resources (VIGMR), 100000 Hanoi, Vietnam.

8 (3) Department of Urban and Environmental Engineering, Liege University, B52- 4000 Liège, Belgium.

9 (4) Department of Civil Engineering, KU Leuven, 3000 Leuven, Belgium.

10 **Corresponding author:** diep.congthi@Ugent.be, Thomas.Hermans@Ugent.be

11 **Abstract.** The lithological and stratigraphical heterogeneity of coastal aquifers has a great
12 influence on saltwater intrusion (SI). This makes it difficult to predict SI pathways and their
13 persistence in time. In this context, electrical resistivity tomography (ERT) and induced
14 polarization (IP) methods are receiving increasing attention regarding the discrimination between
15 saltwater-bearing and clayey sediments. To simplify the interpretation of ERT data, it is commonly
16 assumed that the bulk conductivity mostly depends on the conductivity of pore-filling fluids, while
17 surface conductivity is generally disregarded in the spatial and temporal variability of the aquifers,
18 particularly, once the aquifer is affected by the presence of saltwater. Quantifying salinities based
19 on a simplified petrophysical relationship can lead to misinterpretation in aquifers constituted by
20 clay-rich sediments. In this study, we rely on co-located data from drilled boreholes to formulate
21 petrophysical relationships between bulk and fluid conductivity for clay-bearing and clay-free
22 sediments. First, the sedimentary samples from the drilled wells were classified according to their
23 particle size distribution and analyzed in the lab using a SIP in controlled salinity conditions to
24 derive their formation factors, surface conductivity and chargeability. Second, the deduced
25 thresholds are applied on the field to distinguish clay-bearing sediments from brackish sandy

26 sediments. The results are validated with logging data and direct salinity measurements on water
1 27 samples. We applied the approach along the Luy River Catchment and find that the formation
2
3 28 factors and surface conductivity of the different unconsolidated sedimentary classifications are
4
5 29 varying from 4.0 to 8.9 for coarse-grained sand and clay-bearing mixtures, while normalized
6
7
8 30 chargeability above 1.5 mS/m indicates the presence of clay. The clay-bearing sediments are
9
10 31 mostly distributed in discontinuous small lenses. The assumption of homogenous geological media
11
12 32 is therefore leading to overestimating SI in the heterogeneous clay-bearing aquifers.

13 33 Keywords: aquifer, saltwater intrusion, conductivity, resistivity, induced polarization.

14
15
16 34

1. Introduction

21 35
22
23
24 36 Saltwater intrusion (SI) in coastal aquifers is one of the serious problems that numerous
25
26 37 countries have to face, particularly countries with long coastlines (M. Motallebiana et al., 2019;
27
28 38 H. Ketabchi and M.S. Jahangir, 2021). It has not only a significant local influence through the
29
30 39 degradation of water resources, but it also affects the general development of a country (Insigne
31
32 40 and Kim, 2010; Post et al., 2018). Evaluating the vulnerability of coastal aquifer systems
33
34 41 necessitates a holistic approach encompassing natural elements intertwined with the inherent
35
36 42 characteristics of aquifers, including their geological composition and structure governed by past
37
38 43 climatic and tectonic settings (Y. Changa et al., 2018; Werner et al., 2013; Cong-Thi et al., 2021a;
39
40 44 Dieu et al., 2022). In addition, the anthropogenic influence, through activities such as excessive
41
42 45 groundwater extraction is also crucial (S. Najib et al., 2017; J. A. Mora, et al., 2020; M. Nasiri et
43
44 46 al., 2021).

45 47 In periods of high water level (transgression), the dominant deposition consists of fine-
46
47 48 grained sediments, culminating in the development of clay-rich sedimentary strata. Conversely,
48
49 49 during periods of sea-level decline (regression), previously deposited formations undergo
50
51 50 modification and erosive processes. The coastal sedimentation patterns encompassing alluvial,
52
53 51 aeolian, and lacustrine processes, depending on the hydraulic conditions of the flows, typically
54
55
56
57
58
59
60
61
62
63
64
65

52 lead to the accumulation of sedimentary sequences characterized by a broad range of grain sizes
1 53 (Krumbein, 1934; Krumbein and Sloss, 1963). The succession of numerous regression-
2
3 54 transgression cycles is the main cause of the formation of complex depositional sequences,
4
5 55 resulting in the strong heterogeneity of many coastal aquifers (Koster and Sulter, 1993; Miall,
6
7 56 2000; Ta et al., 2001; Thanh et al., 2017) and a considerable impact on SI existence and
8
9 57 characteristics.
10
11

12
13
14 58 From a hydrogeological perspective, mapping the geometry and physical properties of
15
16 59 aquifers in a coastal setting is a difficult task and requires a large amount of data. Frequently, this
17
18 60 task relies on previously collected geological information pertaining to lithological and
19
20 61 stratigraphic records, but it is time-consuming and lacks reliability when the data are too sparse.
21
22 62 To generate continuous and spatially distributed data, borehole logs can be combined with
23
24 63 geophysical methods (Martínez et al., 2009; Baines et al., 2022). In case of contamination through
25
26 64 SI processes, the task is even more complicated (Cong-Thi et al., 2021a).
27
28
29
30

31 65 Electrical Resistivity Tomography (ERT) is sensitive to the resistivity variations of the
32
33 66 subsurface which depends on the pore-filling fluid and lithology. Recovering the lithological
34
35 67 heterogeneity of coastal aquifers from ERT is a challenging task, particularly in saline conditions
36
37 68 because low resistivity values can be attributed to either brackish-salt water or clay-rich sediments
38
39 69 or both (Nguyen et al., 2009; Tassy et al., 2019). To estimate the salinity from the bulk resistivity
40
41 70 distribution, the most common approach is to use Archie's law (Archie, 1942). It calculates the
42
43 71 formation factor (F) which is the ratio between the conductivity of pore fluids and that of the
44
45 72 porous medium. The role of surface conductivity related to the electrical double layer (EDL) is
46
47 73 ignored. However, the latter contributes significantly to the increased conductivity in the presence
48
49 74 of clay (Waxman and Smits, 1968; Vinegar and Waxman, 1984; Revil and Skold, 2011; Revil et
50
51 75 al., 2017). Although the pore fluid effect is dominant in high salinity environments, allowing to
52
53 76 map saline zones with relative certainty, the surface conductivity effect prevents the identification
54
55
56
57
58
59
60
61
62
63
64
65

77 of freshwater resources when clay is present, as they can be easily misinterpreted as brackish zone
78 (Szalai et al., 2009; Michael et al., 2016; Cong-Thi et al., 2021a).

79 Induced polarization (IP) measures the ability of the subsurface to store electrical charge
80 under the impact of an electric field (Marshall et al., 1959). Time-Domain IP (TDIP) surveys are
81 conducted similarly to ERT surveys, by sending a current into the ground while measuring the
82 resulting potential difference. After shutting the current off, the potential decay in the subsurface
83 is measured in several time windows to characterize its chargeability, which is the ratio of the
84 secondary voltage (decay) over the primary voltage of the transmitted current. Dividing the
85 chargeability by the resistivity results in the normalized chargeability that might highlight zones
86 with high surface conductive properties (Magnusson et al., 2010; Slater et al., 2002) such as clay-
87 rich media. Higher normalized chargeability is expected in clay-rich sediments while coarser-
88 grained soils including sand, gravel, and grit commonly yield lower values (Alabi et al., 2010). IP
89 surveys have proven to be an effective tool for mapping the lithological layers of unconsolidated
90 sediments, in particular the presence of clay content (Benoit et al., 2019). However, TDIP has a
91 low signal-to-noise ratio and is therefore sensitive to noise (Dahlin et al., 2002; Dahlin et al., 2012).
92 Combined with the weak signals linked to high conductivity measured in saline conditions, it
93 makes the method quite challenging to apply for SI studies (Attwa et al., 2011).

94 An additional alternating approach at the laboratory scale is spectral induced polarization
95 (SIP) measurement. It measures the complex conductivity of the subsurface at various frequencies.
96 SIP is considered as the optimum solution to characterize the interfacial polarization at the
97 interface between materials and pore-filling fluids (D. Korošak et al, 2007; Revil and Florsch 2010;
98 Revil and Skold, 2011), contributing to the complex conductivity of porous materials. If the
99 dependence of the complex conductivity on the mentioned-above factors is dissected, it will help
100 to distinguish the origin of conductive anomalies (Waxman and Smits, 1968; Vinegar and
101 Waxman, 1984; Revil and Skold, 2011).

102 In a previous study, Cong-Thi et al., (2021a) qualitatively delimited the extent of saltwater
1 103 intrusion in the Luy River catchment using ERT. However, in the absence of co-located data, their
2
3 104 method was based on the identification of the response of clay in freshwater conditions.
4
5 105 Intermediate values of resistivity could not be unequivocally interpreted as they could correspond
6
7
8 106 to clay-rich or brackish water zones.
9

10
11 107 The objective of this study is to develop a methodology combining laboratory and field
12
13 108 measurements to characterize the petrophysical relationship in heterogeneous aquifer based on co-
14
15 109 located data. The discrepancy of resistivity values controlled by the presence of clay minerals and
16
17
18 110 salinity is identified using the lithological and hydrological information. Firstly, the co-located
19
20 111 sedimentary samples are classified through particle size distribution analysis (PSD). Secondly, the
21
22 112 petrophysical relationship for different grain-sized patterns is estimated based on spectral induced
23
24
25 113 polarization (SIP). Lastly, the validity of the laboratory petrophysical relationship at the field scale
26
27 114 is assessed by comparing ERT and TDIP data with high-resolution logs and total dissolved solids
28
29 115 (TDS) content from water samples. The methodology is applied to better characterize the
30
31 116 heterogeneity and salinity of the coastal aquifer of the Luy River catchment, Vietnam.
32
33
34
35

36 117 **2. Study area**

37
38
39

40 118 The Luy River catchment is located in Binh Thuan, a Southern Central province in Vietnam
41
42 119 (Fig. 1), and is governed by a complex geological and tectonic context. Terrains on both sides of
43
44 120 the river are quite different: low plains dominate on the left bank, while huge sand dunes are
45
46 121 present on the opposite bank. Along the Luy River, the unconsolidated sedimentary sequences
47
48 122 formed during both the Pleistocene and Holocene periods are discontinuously present in various
49
50 123 thicknesses. The Pleistocene sediments were deposited during successively transgressive and
51
52 124 regressive stages (Hoang Phuong, 1997). Our lithostratigraphic data recorded in the borehole logs
53
54
55 125 shows that the Pleistocene layers have a low thickness on the left bank, while they are relatively
56
57
58 126 thick on the right bank (Cong-Thi et al., 2021b). Sediments derived from marine-alluvial sources
59
60 127 (Hoang Phuong, 1997; Cong-Thi et al., 2021a) are composed of clean sand, clay, clayey sand
61
62
63
64
65

128 sometimes containing grits, gravels, and small rocky fragments derived from pre-host rocks. Well-
 129 rounded quartz dominates while feldspar and other minerals (ilmenite, limonite, mica) are present
 130 as minor components in the lithological units (Cong-Thi et al., 2021b).

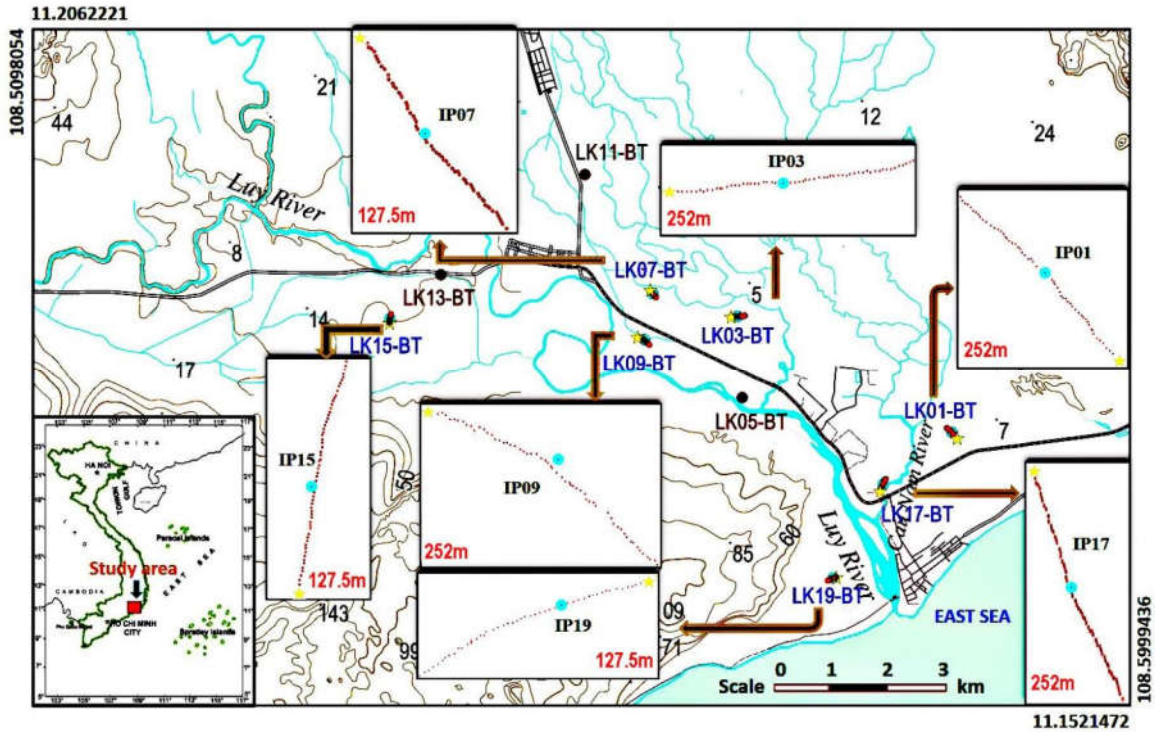


Figure 1: Location of the study site. Boreholes are indicated by brown and blue circles. Geophysical measurements coincide with the green boreholes. Yellow stars indicate the first electrode in geophysical lines whose lengths are specified in red. The analyzed unconsolidated samples were collected from these boreholes.

131 The Holocene sediments were dominantly accumulated through the Flandrian
 132 transgression during the Early-Middle Holocene and regression in the Middle-Late Holocene
 133 (Hoang Phuong, 1997; Tran Nghi et al., 2007). The former is supported by the profile of LK07-BT
 134 and LK13-BT (Fig. 1) with the grain size decreasing gradually from clay-bearing coarser sand
 135 close to the bedrock to fine clayey sand near the surface (Cong-Thi et al., 2021b). The latter is
 136 proven by grain-sized descriptions of LK01-BT, LK17-BT, and LK19-BT. The Holocene layer
 137 with a thickness of 2 m to 20 m is characterized by alternating sedimentary layers of varying
 138 compositions such as sandy layers with interbedded clayey sand, and sandy clay layers, sometimes

139 including fine-grained silt. The lithological composition including arkose and lithic-arkose sand
140 was possibly connected to the sandy debris derived from the magmatic arcs, subduction complex,
141 and eroded granitoid in the older tectonic setting (Dickinson, 1979; Miall, 2009) and
142 complemented by deposition formed in lagoons that were forming a group of alluvial-marine
143 transition facies (Nguyen Van Vuong, 1991; Hoang Phuong, 1997). Moreover, the local presence
144 of multi-colored clay lenses forming locally aquitard units and containing black humus is
145 characteristic of this period.

146 The transgressive and regressive cycles induced repeated sea-level changes combining
147 depositional and erosional effects, and sedimentary discontinuity, resulting in lowstand,
148 transgressive, and highstand systems tracts (LST, TST, HST respectively) (Tran Nghi et al., 2007).
149 Obviously, the sea-level changes played a vital role in the variation of the sedimentary
150 compositions and the presence of seawater in aquifers. Recent hydrogeological investigations
151 revealed that the aquifer system is experiencing a long-term freshening trend, likely since the last
152 water highstand, but is locally affected by salinization resulting from anthropic activities (Dieu et
153 al., 2022). Paleo-seawater has been entrapped in the clay-rich sediments, the heterogeneous nature
154 of sediments therefore plays a major role in the distribution of salinity in the study area (Dieu et
155 al., 2022).

156 **3. Methodology**

157 **3.1. Laboratory measurement**

158 *3.1.1. SIP measurement configuration*

159 To scrutinize the petrophysical relationships of the porous sediments, the complex
160 electrical conductivity of various grain-sized categories is first investigated at the laboratory scale
161 through SIP measurements. We rely on the SIP system proposed by Zimmermann et al. (2008)
162 using the four-point measurement method represented by two electrodes for current injection and
163 two other electrodes for potential differences (Appendix A). A polyvinyl chloride sample holder

164 32 cm long with a 3 cm inner diameter was employed. The potential (brass) electrodes were spaced
1 165 12.5 cm from the current electrodes, 7 cm apart (twice the inner diameter of the sample holder),
2
3 166 and retracted from the sample to reduce polarization effects and phase errors to the resolution limit
4
5
6 167 of the system (< 0.1 mrad below 1 kHz, (Zimmermann et al., 2008; Revil and Skold, 2011)).
7
8 168 Current electrodes were inserted across the whole section perpendicular to the main axis of the
9
10
11 169 sample holder. In order to further reduce phase inaccuracy, we verified that the contact impedance
12
13 170 was smaller than the sample impedance (Zimmermann et al., 2008).
14
15

16 171 Two separate procedures are used for the clay-free and clay-bearing samples. Clean sand
17
18 172 with natural moisture was compacted into the sample holder to obtain a homogenous density. The
19
20
21 173 filled sample column was fully saturated under five different electrolytes (NaCl solution) of
22
23 174 respective conductivity 2.59 mS.m^{-1} , 25.2 mS.m^{-1} , 392 mS.m^{-1} , 1793 mS.m^{-1} , and 5560 mS.m^{-1}
24
25
26 175 corresponding to deionized, fresh, slightly brackish, brackish, and saline water respectively. The
27
28 176 three first solutions correspond to low and moderate salinity conditions while the two remaining
29
30
31 177 values represent higher saline conditions. To avoid the effect of the accumulative salts stemming
32
33 178 from the earlier saturation, the measurements were performed from the lowest to the highest
34
35
36 179 salinity. Water was injected into the sample until the electrical conductivity of the output water
37
38 180 was stable and in equilibrium with that of the input. For clay-bearing mixtures having clay content
39
40
41 181 from 15% to 35%, water injection within the column was impossible because of the low
42
43 182 permeability of the sample. Therefore, we saturated the sample with the respective solutions before
44
45 183 inserting them into the sample column.
46
47

48 184 In addition, the recorded electrical conductivity values were also corrected for temperature
49
50
51 185 (Hayasi et al., 2004; Hermans et al., 2014; Hermans et al., 2015) to 20°C , considering a 2%
52
53 186 increase of electrical conductivity per degree Celsius.
54
55

$$\sigma_{20^\circ\text{C}} = \frac{\sigma_{rec}}{1+0.02(t_{rec}-20)} \quad (1)$$

56
57
58
59
60
61
62
63
64
65

187 where σ_{rec} (in $\text{S}\cdot\text{m}^{-1}$) is the electrical conductivity recorded in saturated conditions of the
1 188 temperature t_{rec} ($^{\circ}\text{C}$) and $\sigma_{20^{\circ}\text{C}}$ (in $\text{S}\cdot\text{m}^{-1}$) is the corrected electrical conductivity at 20°C .

2
3
4 189 The complex conductivity and phase shift are investigated at the voltage of 5 V and the
5
6 190 frequency in an interval range from 1 Hz to 45000 Hz. However, during processing, we prioritize
7
8
9 191 the low-frequency range under 1000 Hz, particularly at 1 Hz due to their stability and sensitivity
10
11 192 to salinity. For all salinities, three replicates were investigated. We also measured both reciprocal
12
13
14 193 and normal measurements to estimate the error. The reciprocal measurements were performed
15
16 194 prior to normal measurements. A reciprocal measurement is a procedure where current and
17
18
19 195 potential electrodes are switched. The voltage difference applied during the reciprocal
20
21 196 measurement was of lower intensity to stay close enough to the current-free electrode impedance.
22
23 197 It was usually ± 0.1 V instead of ± 5 V (Huisman et al., 2016).

24
25
26 198 An essential point in the evaluation of the complex electrical conductivity is the assessment
27
28
29 199 of the geometrical factor of the sample holder (Revil et al., 2017). To translate a measured complex
30
31 200 impedance to a complex electrical conductivity, this factor depends on the position of electrodes
32
33
34 201 which affects the current distribution between the current electrodes and the geometry of the
35
36 202 sample holder. We determined the geometric factor by filling the column with the saline solutions
37
38
39 203 of known conductivity only (no solid matrix) and measuring the impedance with the mentioned-
40
41 204 above SIP configuration. The geometrical factor of our sample holder is 0.01357 m.

42 43 44 205 *3.1.2. Sample preparation*

45
46
47 206 Particle size distribution analysis (PSD) (Wentworth, 1922) using both wet and dry standard
48
49 207 sieving techniques as stipulated in the American Society for Testing and Materials (ASTM D422-
50
51 208 63) was first applied to sort unconsolidated sediments. Fifty-five disturbed samples collected from
52
53
54 209 ten drilled boreholes coinciding with the geophysical measurements (Fig. 1) were classified into
55
56
57 210 four groups: three clay-free categories composed of clean sand (fine-, medium-, and coarse-
58
59 211 grained sand) and a clay-bearing mixture category. In addition, the finer suspended particles of the
60
61 212 $2\ \mu\text{m}$ fraction were analyzed through X-ray diffraction revealing the mineralogical content of the
62
63
64
65

213 clay fraction mainly contains an aggregate of kaolinite, illite, chlorite, and a smaller quantity of
 1 214 goethite (Table 1).

215 Table 1: Summary of the results of X-ray diffractograms

Order. No	Sample. No	Mass (gram)	Components and content (%)						
			<i>Illite</i>	<i>Kaolinite</i>	<i>Chlorite</i>	<i>Quartz</i>	<i>Potassium Feldspar</i>	<i>Goethite</i>	<i>Others</i>
1.	LK07-BT (0-13m)	58.31	18-20	7-9	1-3	51-53	9-11	4-6	-
2.	LK07-BT (13-15m)	58.46	15-17	12-14	3-5	48-50	8-10	3-5	Amphibole, Lepidolite, Calcite

216 3.1.3. Complex conductivity (σ)

217 Complex conductivity (σ) can be expressed as :

$$\sigma(\omega) = \sigma'(\omega) + i\sigma''(\omega) = |\sigma|e^{i\varphi} \quad (2)$$

218 with $|\sigma| = \sqrt{\sigma'^2 + \sigma''^2}$ the amplitude, $\varphi = \text{atan} \frac{\sigma''}{\sigma'}$ the phase shift, σ' the real or in-phase
 219 component related to the ohmic conduction properties and σ'' the imaginary or out-of-phase
 220 component linked with the capacitive and inductive properties. For small phase shifts as the ones
 221 observed for consolidated and porous sediments (<100 mrad), phase shifts can be estimated as the
 222 ratios:

$$\varphi_r(\omega) \approx \left(\frac{\sigma''(\omega)}{\sigma'(\omega)} \right) \quad (3)$$

223 This approximation is fairly valid for metal-free soils and rocks (Kemna, 2000; Schön, 2011;
 224 Heenan et al., 2013; Saneiyani et al., 2018).

225 At low frequencies comparable to field surveys of time-domain IP (<10 Hz), we may
 226 neglect the effect of the complex permittivity ε^* so that the effective in-phase conductivity and the
 227 effective quadrature conductivity corresponds to σ' and σ'' (Kremer et al., 2016). For higher

228 frequencies, the displacement current has to be taken into account through the dielectric
1 229 permittivity.

2
3
4 230 When electronic semi-conduction or metallic conduction can be neglected, i.e. in the
5
6 231 absence of metal-bearing grains, the conductivity may be described in terms of the electrolyte
7
8
9 232 conduction σ_{el} , which may be regarded as affecting only the real part of conductivity in parallel
10
11 233 with interfacial or surface conduction (σ_{int}), which affect both the real and the imaginary parts of
12
13
14 234 conductivity (Kemna, 2000).

$$\sigma = \sigma_{el} + \sigma_{int} \quad (4)$$

15
16
17
18
19 235 Archie's law can be used to empirically quantify the electrolytic conduction σ_{el} (Archie,
20
21 236 1942; Schön, 2011), which for a saturated medium is given by:

$$\sigma_{el} = \frac{\sigma_f}{F} = \frac{\Phi^m}{a} \sigma_f \quad (5)$$

22
23
24
25
26
27
28
29 237 The formation factor ($F = \frac{a}{\Phi^m}$) is also inversely proportional to pore textural properties,
30
31
32 238 namely the cementation exponent (m) and porosity (Φ) (Schön, 2011), while a is an empirical
33
34
35 239 factor that should be equal to one and σ_f the pore fluid conductivity.

36
37
38 240 The complex interfacial conductivity can be expressed for a saturated medium as (Börner
39
40 241 et al., 1996):

$$\sigma_{int} = \frac{h(\sigma_f) S_{por}}{F} (1 + il) \quad (6)$$

41
42
43
44
45
46
47 242 where $h(\sigma_f)$ is a nonlinear real function of salinity, S_{por} refers to the specific surface area
48
49
50 243 related to pore volume. The parameter $l = Im(\sigma_{int}) / Re(\sigma_{int})$ accounts for the actual separation
51
52 244 of σ_{int} into real and imaginary parts and generally varies from 0.01 to 0.15 (Börner et al., 1996).
53
54
55 245 Since the σ_{el} is a real quantity, the interfacial properties can be accessed through the imaginary
56
57 246 part of σ'' which depends on $Im(\sigma_{int})$ whereas the real part of σ' relates to both σ_{el} and σ_{int} . As
58
59
60 247 σ_f decreases and tends towards zero, the real part of σ' may allow to access the real part of the σ_{int} .

61
62
63
64
65

It is standard to fit a Cole-Cole model to relate the induced polarization effects in the time domain with the observations in the frequency domain (Everett, 1997). Indeed, the Cole-Cole model is an accepted complex conductivity/resistivity model expressed by the normalized chargeability (M_n), the frequency dependence (f or ω), and the time constant (τ) (Kemna, 2000) as follows:

$$\sigma_c = \sigma_\infty - \frac{M_n}{1 + (i\omega\tau_0)^c} \quad (7)$$

$$M_n = \sigma_\infty - \sigma_0 \geq 0$$

where M_n defines the normalized chargeability, c refers to the frequency exponent ($0 \leq c \leq 1$), τ_0 represents the relaxation time (or time constant) in seconds and σ_0 and σ_∞ define the electrical conductivity at low frequency and high frequency, respectively. In addition, M_n is a function of the conductivity (σ'') in the imaginary part.

Following the methodology of Revil (2017), the normalized chargeability is correlated with the quadrature conductivity measured at (or close to) the relaxation peak.

$$\sigma'' = -\frac{1}{2} \frac{M_n \cos[\frac{\pi}{2}(1-c)]}{\cosh[c \ln(\omega\tau_0)] + \sin[\frac{\pi}{2}(1-c)]} \quad (8)$$

At the critical frequency $\omega = 1/\tau_0$, $0 \leq c \leq 1$ and with c fixed to 0.5 for uniform ranges of grain-sized particles and smaller for broad sizes, σ'' is intimately related to M_n by:

$$\sigma'' = -\frac{1}{2} \frac{M_n \cos[\frac{\pi}{2}(1-c)]}{\cosh[c \ln(\omega\tau_0)] + \sin[\frac{\pi}{2}(1-c)]} \quad (9)$$

$$\sigma'' = -\frac{1}{2} \frac{\cos[\frac{\pi}{2}(1-c)]}{\sin[\frac{\pi}{2}(1-c)]} M_n \quad (10)$$

$$\sigma'' = -\frac{1}{2} \left(\frac{\sqrt{2}}{1+\sqrt{2}} \right) M_n \approx -\frac{1}{5} M_n \quad (11)$$

1
2
3
4
5
6
7
8
9
10
11
12
13
14
15
16
17
18
19
20
21
22
23
24
25
26
27
28
29
30
31
32
33
34
35
36
37
38
39
40
41
42
43
44
45
46
47
48
49
50
51
52
53
54
55
56
57
58
59
60
61
62
63
64
65

262 M_n is considered to be approximate 5 times σ'' (Revil et al., 2015). In other words, M_n is not only
263 quantified by the intensity of surface polarization but is also proportional to σ'' .

264 3.2. Field measurement

265 3.2.1. ERT and TDIP measurements

266 ERT and TDIP imaging were performed on 7 profiles collected in both upstream and
267 downstream parts along the Luy River. All mid-points of profiles coincide with the boreholes
268 where the samples for laboratory analysis were collected (Fig. 1).

269 With the goal of validating the petrophysical relationship accounting for clay and obtaining
270 a good signal-to-noise ratio, the ABEM Terrameter LS1 equipment using dipole-dipole
271 configuration including 64 electrodes was used in each profile with 2.5 m and 4 m separation
272 between electrodes depending on the depth of the drilled boreholes. The minimum and maximum
273 currents were 10 mA and 500 mA respectively. The acquisition delay time was set up at 0.8 seconds
274 and the acquisition time to 1.2 seconds resulting in a total injection of 2 seconds. The TDIP signal
275 was recorded using 20 time windows using increasing time intervals for a total recording time of
276 4.0 seconds. To reduce the contact resistance and maintain a reliable signal-to-noise ratio
277 throughout the investigation sequences, saltwater was poured at the locations of the electrodes
278 buried under dry sand conditions. The acquisition protocol was sorted to avoid the electrode
279 polarization effect (Dahlin et al., 2002).

280 Prior to inversion, the negative resistance values and chargeability exceeding 1000 mV/V,
281 that are considered physically impossible (Loke, 2011) were removed, and noisy decay curves
282 were removed manually (Evrard et al., 2018). Relying on the methodology proposed by Slater et
283 al. (2000), data quality was also assessed for 6 profiles based on reciprocal measurements. A
284 threshold of 1% was selected to filter the data sets for all profiles, except for the reciprocal error
285 in profile LK19-BT, for which 5% was selected. The dataset is inverted in RES2DINV (Loke and

286 Baker, 1996). The L1-norm was used for both the model constraint to promote sharper resistivity
1 287 contrasts (Cong-Thi et al., 2021a) and the data constraint to limit the impact of possibly remaining
2
3 288 outliers.
4

6 289 3.2.2. *Electromagnetic logs* 7 8

9 290 Electromagnetic induction (EM-log, Geonics©) was used to collect vertically detailed logs
10
11 291 of the electrical conductivity in 9 drilled boreholes equipped with non-conductive PVC casing
12
13 292 (Vandenbohede et al., 2008). The probe operates at a frequency of 39.2 kHz with a coil spacing of
14
15 293 0.5 m (Mc Neill, 1990).
16
17
18

19 294 Before each logging, the calibration procedures were applied to verify that the probe was
20
21 295 solely measuring zero conductivity. Data were collected in the vertical direction using a distance
22
23 296 interval of 0.2 m. The collected data were validated in both up and down directions. The inner
24
25 297 diameter of the boreholes is 60 mm to minimize the influence of the borehole fluid and casing, as
26
27 298 the probe's sensitivity is maximum at a radial distance of 30 cm from the probe center (McNeil et
28
29
30
31 299 al., 1990).
32
33
34

35 300 **4. Results** 36 37

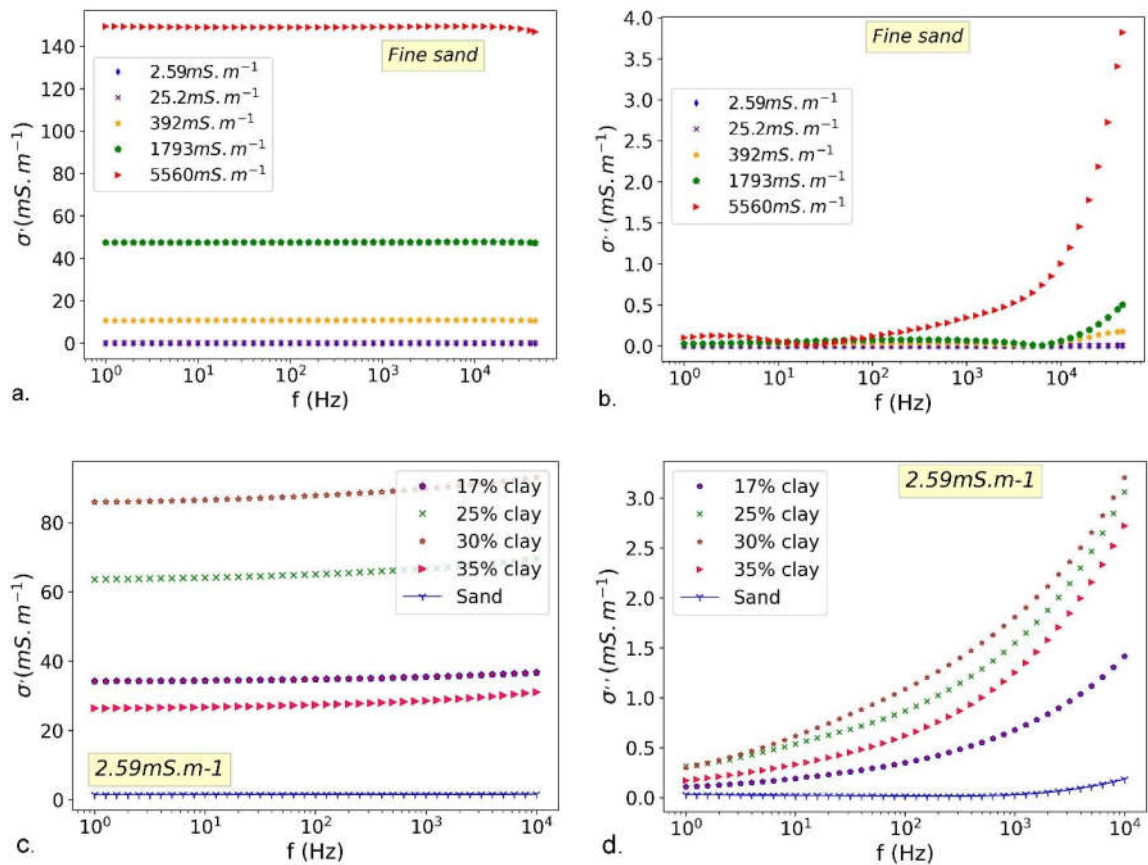
38 301 **4.1. Laboratory results** 39 40

41 302 *4.1.1. SIP* 42 43

44 303 Figures 2a and b show a significant influence of the NaCl concentration on the spectra of
45
46 304 both real (σ') and imaginary (σ'') conductivity. Besides, the dependence of the out-of-phase
47
48 305 component is simultaneously observed at a higher frequency of 1000 Hz (Fig. 2b). As expected,
49
50 306 higher saline concentration corresponds to higher magnitudes of complex conductivity (Fig. 2a),
51
52 307 whereas the opposite trend is observed for the phase (Appendix B). In addition, no peak is observed
53
54
55 308 in the complex conductivity spectra. This might be explained by the non-uniform grain size of the
56
57
58 309 sandy materials. Figure 2c and d illustrate the influence of the presence of clay minerals, increasing
59
60
61
62
63
64
65

310 both the real and imaginary conductivity components, particularly for low salinity. This increase
 1 311 is dependent on the clay content of the samples.

2
 3
 4 312 The sample containing 35% has a lower conductivity than expected, this could be caused
 5
 6 313 by an increase in the cementation exponent. Natural clay in sediments can play a considerable role
 7
 8
 9 314 as cement in the pore space of sandy sediments, resulting in reducing the porosity and pore-
 10
 11 315 connectivity, particularly surface ionic mobility. Furthermore, the surface conductivity caused by
 12
 13
 14 316 charged ion mobility in the EDL dominates the complex conductivity. This phenomenon also
 15
 16 317 affects the quadrature conductivity component. In other words, the mixture containing a large
 17
 18
 19 318 proportion of clay minerals seems to be more compacted, reducing the cation exchange capacity
 20
 21 319 (CEC) of clay. This effect might have been induced by the sample preparation.



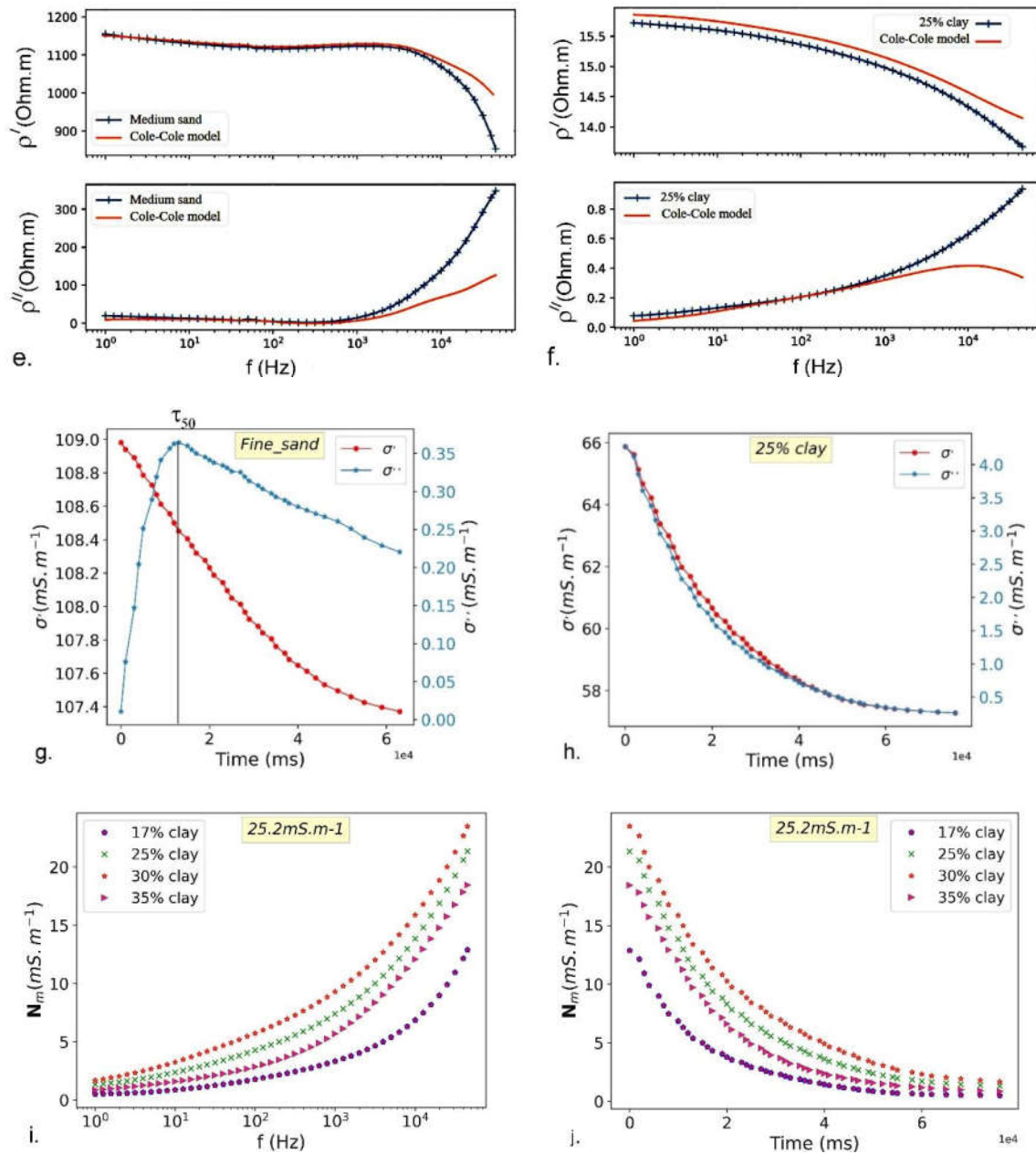


Figure 2. a. The in-phase (σ') and b. out-of-phase (σ'') conductivity components of the representative clean sand category for different salinities. Effects of clay content with respect to the surface conductivity at the lowest salinity, corresponding to deionized water on the amplitude of the in-phase (c) and out-of-phase components (d). Fitting with the Cole-Cole model for fine sand (e) for 25% clay-bearing sand (f). The peak of the synthetic SIP data in terms of real and quadrature conductivity, for fine sand (g) and clay-bearing sand (h). Normalized chargeability against frequency (i) and time (j).

320

The Cole-Cole model approach was used to fit the measured SIP curves of all clay-free

321

and clay-bearing categories using PyGIMLi. Figures 2e and 2f show the IP spectra of the

322 representative samples for fine sand and clayey sand (25% clay), with the c exponent equal to 0.5.
1 323 The decomposition fits the curve of fine sand more accurately than that of the clay-bearing sample.
2
3 324 For the imaginary component, except for the well-fitted spectra of the quadrature component under
4
5
6 325 1000 Hz, a partition of the spectra is not well-fitted by the Cole-Cole model at frequencies above
7
8 326 1000 Hz. The reason could be the potential effect of the roughness of the grains in polarization
9
10
11 327 conditions of the grain-pore water interface and the dielectric effect (Leroy et al., 2008; Revil,
12
13 328 2014).

16 329 Figure 2g and 2h illustrate the two-phase component spectra of real and quadrature
17
18
19 330 conductivity on time scales. A peak is observed in the spectrum of the fine sand sample in a time
20
21 331 interval of 1-2 ms, which is the relaxation time τ_{50} at which 50 percent of the total chargeability is
22
23 332 reached (Weigand and Kemna, 2016). Inversely, no clear dominant relaxation time is observed for
24
25
26 333 the broad grain-sized clay-bearing sample. As mentioned earlier, this might be associated with the
27
28 334 surface roughness effects and the superposition of particles, widening the relaxation time (Sara
29
30
31 335 Johansson, 2020).

34 336 The normalized chargeability is also plotted against frequency and time as cumulative
35
36 337 curves (Eq. 11, Fig. 2i and j). The normalized chargeability varies proportionally with the
37
38
39 338 increased clay content. For the low-frequency range around 1 Hz, a threshold value for the
40
41 339 normalized chargeability around $1.5 \text{ mS}\cdot\text{m}^{-1}$ can be deduced to validate the presence of clay.

44 340 *4.1.2. Petrophysical relationship*

47 341 To estimate the relation between the real conductivity, the pore fluid conductivity and the
48
49 342 interfacial conductivity, we rely on equations 4 and 5. Figure 3a shows two different trends for
50
51
52 343 clay-bearing and clay-free samples. For the clean sand category, a nearly linear dependence of the
53
54 344 in-phase conductivity on the pore water conductivity is observed. Inversely, a non-linear
55
56
57 345 relationship is clearly observed in the clay-bearing mixtures, particularly for low salinities where
58
59 346 surface conductivity even dominates due to mobile ions in the EDL. The general tendency of the
60
61
62 347 relationship observed is a linear portion at high salinity with a non-linear transition at lower
63
64
65

348 salinities where the curve approximately approaches a constant, which represents the surface
 1 349 conductivity at low salinity.

350 The increased clay content in the range 17%-30% yields a growing influence of the surface
 6 351 conductive values on the amplitude of the intercept as observed in Fig. 3b. The sample with 35%
 9 352 clay does not follow this trend as explained above.

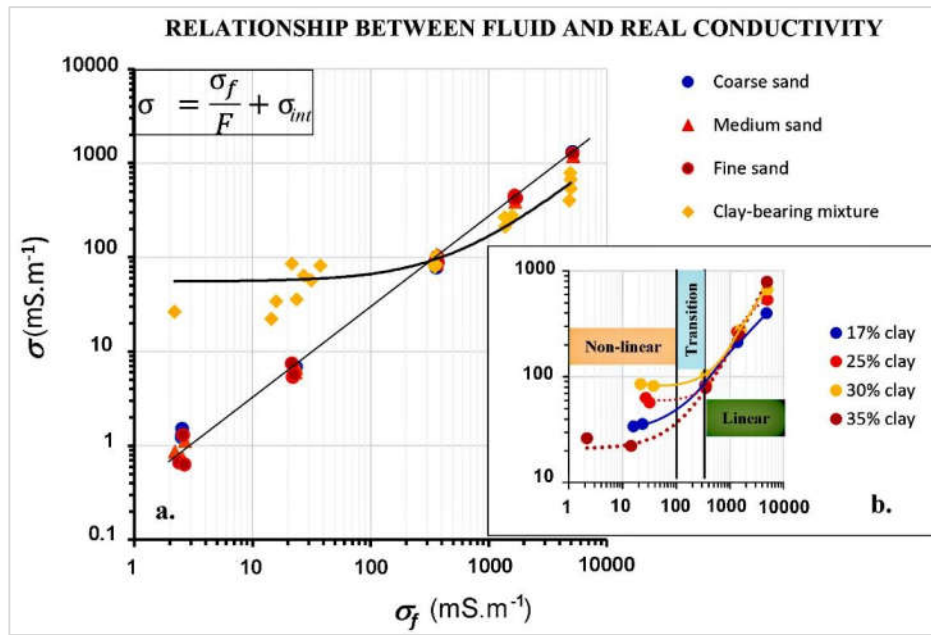


Figure 3. Log-log plot of the pore fluid conductivity versus the real conductivity. (a). A straight line represents the clean sand category (including coarse-, medium- and fine particles) and a curve refers to the clay-bearing mixture. (b). The generally detailed trends between σ and σ_f of four clay-bearing samples indicate linear relationships at higher salinity and non-linear relationships at lower salinity.

353 The formation factor F is the reciprocal of the slope in the linear portion, and the surface
 354 conductivity σ_{int} is the intercept part. (Table 2). The surface conductivity of clay-bearing sand is
 355 up to 40 times larger than that of clay-free sediments.

356 Table 2. Formation factor and surface conductivity of four sedimentary groups in the Luy River

Category		F	σ_{int} (mS.m^{-1})
Clay-free sediments	Coarse sand	4	2
	Medium sand	4.4	6

	Fine sand	4.1	5
Clay-bearing sediments	17% clay	13.4	55
	25% clay	10.3	71
	30% clay	8.3	76
	35% clay	6.4	21
	Mean	8.9	55

Based on the petrophysical relationship, it is possible to define resistivity threshold values corresponding to freshwater and saline water transitions (based on 1000 and 3000 mg/L TDS limits, Cong-Thi et al., 2021a) for the four porous sediment groups calculated using equations 4 and 5 and the fitted parameters. Water electrical conductivity is converted into TDS values using a linear relationship (Keller et al., 1966; Cong-Thi et al., 2021a). Due to the uncertainty in the formation factor resulting from the different samples, we use conservative rounded threshold values (Table 3). For the sand categories, resistivity under 9 Ohm.m corresponds to saline conditions (> 3000 mg/L), and resistivity above 25 Ohm.m indicates freshwater (< 1000 mg/L). The intermediate interval corresponds to brackish water. Analogously, the threshold values for the clay-bearing mixture are 9 Ohm.m and 14 Ohm.m for saline and freshwater conditions respectively. Remarkably, these values are in agreement with the estimation of Cong-Thi et al., (2021a) made in the absence of co-located data. The threshold to be used for freshwater depends on the normalized chargeability (14 Ohm.m if $M_n > 1.5$ mS.m⁻¹, 25 Ohm.m otherwise).

Table 3. Resistive threshold values for the Luy River sediments in different salinity conditions

Category	Resistivity threshold (Ohm.m)	Condition
Clay-free sediments	>25	Fresh
	9-25	Brackish
	<9	Saline

Clay-bearing sediments	>14	Fresh
	9-14	Brackish
	<9	Saline

1
2
3
4
5
6
7
8
9
10
11
12
13
14
15
16
17
18
19
20
21
22
23
24
25
26
27
28
29
30
31
32
33
34
35
36
37
38
39
40
41
42
43
44
45
46
47
48
49
50
51
52
53
54
55
56
57
58
59
60
61
62
63
64
65

371 **4.2. Field results**

372 *4.2.1. Resistivity and TDIP*

373 Assuming that laboratory samples are representative for field conditions, the threshold
374 values computed at the laboratory scale can be used for the field scale interpretation, and combined
375 with borehole logs to characterize the complex distribution of heterogeneous sediment sequences.
376 Examples are given in Fig. 4 and 5 for two selected profiles (IP07 and IP03). Near the surface,
377 since unsaturated and freshwater conditions dominate, the observed resistivity varies laterally from
378 5 Ohm.m to 45 Ohm.m in both profiles, indicating clay-dominated lithology as confirmed by the
379 respective lithologs (LK07-BT and LK03-BT). Deeper, in IP07 lower resistivity values varying
380 from 1.5 Ohm.m to 3 Ohm.m are visible at depths from 5 m to 14 m. The lithology is relatively
381 homogeneous, corresponding to sandy clay under saline conditions. The high values of the
382 normalized chargeability observed at the bottom of the borehole in IP07 might be related to the
383 high clay content along the whole litholog although the presence of artefacts of inversion is
384 possible given the amplitude of the anomaly. Nevertheless, normalized chargeability higher than
385 1.5 mS.m are consistently observed along the first half of the profile.

386 In IP03, a decrease of resistivity values at depths between 3 m and 15 m from 16 Ohm.m
387 to 4 Ohm.m from the right part to the left part of the figure seems inversely proportional to the
388 higher clay content, as corroborated by the higher normalized chargeability from 3 mS.m⁻¹ to
389 approximately 4.5 mS.m⁻¹. This reveals that surface conduction mechanisms of disseminated clay
390 particles play a significant role in low resistivity.

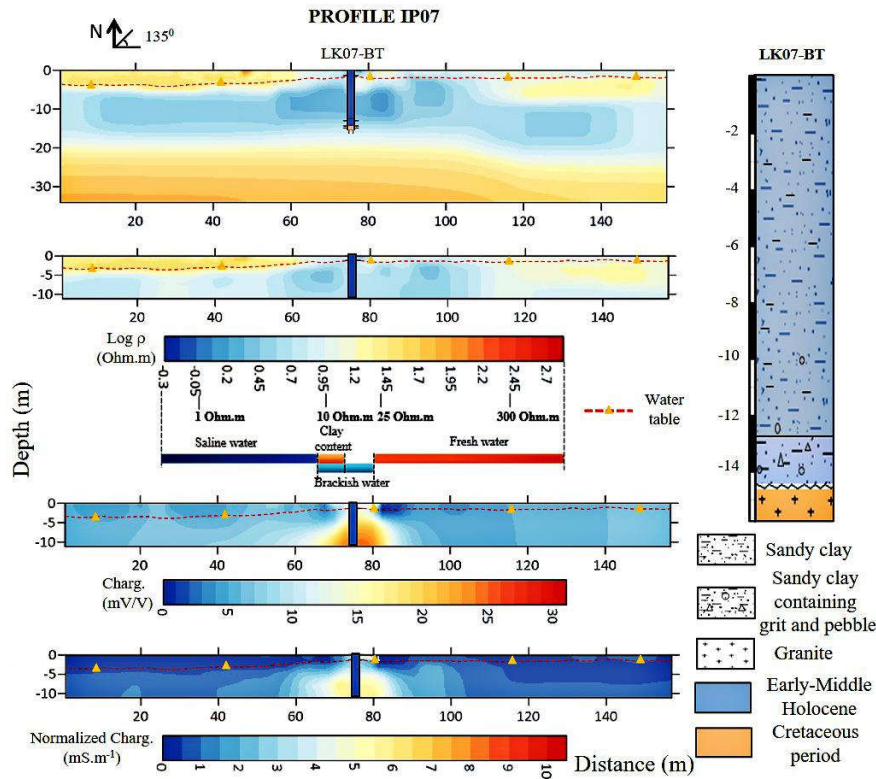


Figure 4: Inverted resistivity, chargeability and normalized chargeability of IP07 in correlation with lithostratigraphical logs in boreholes LK07-BT. Lower is the mapping of chargeability/ normalized chargeability. The broad variation of chargeability in profiles shows the more complicated distribution of clay content in the inhomogeneous context of lithology. Root-mean-squared (RMS) errors of IP07 chosen at 5 consecutive iterations are 1.28% and 0.96% in resistivity inversion and in chargeability map, respectively.

391 The transition between the unconsolidated sediment layers and unaltered bedrock is
 392 characterized by the rapid increase of resistivity ranging from 50 Ohm.m to 150 Ohm.m. For both
 393 profiles, the bedrock is identified as expected by an increase in resistivity. The discrepancy in the
 394 depth is likely linked to the smoothing effect of inversion (Cong-Thi et al., 2021a).

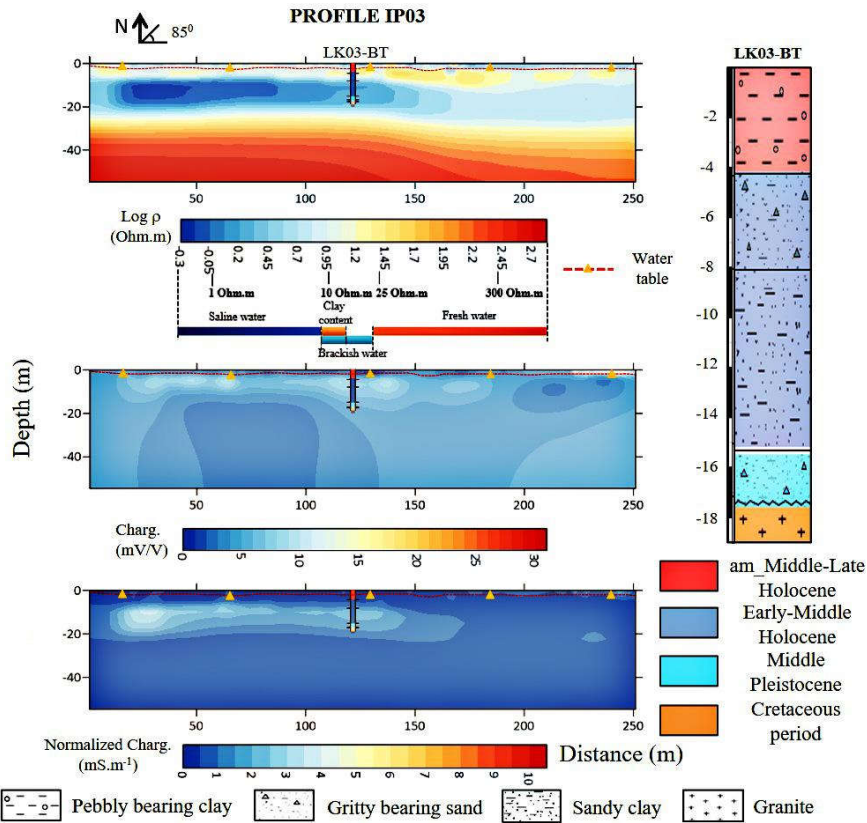


Figure 5: Similar to IP07, the inverted resistivity, chargeability and normalized chargeability of IP03 in correlation with lithostratigraphical logs in boreholes LK03-BT. Lower is the mapping of chargeability/normalized chargeability. Higher normalized chargeability indicates the presence of clay content. Root-mean-squared (RMS) errors of IP03 chosen at 5 consecutive iterations is 0.97% and 0.44% in resistivity inversion and in chargeability maps, respectively.

4.2.2. Correlation between EM-logs and ERT data

To validate the variations of the resistivity in the heterogeneous sediment layers, we provide a comparison of the inverse solutions with co-located data by computing the average recorded value in EM-logs within the corresponding ERT grid cells. Averaging within a grid cell allows to partly account for the different investigated volumes (Benoit et al., 2019).

Overall, ERT can reproduce relatively well the conductivity trend measured in logs (Fig. 6 and 7). Better matching between both measuring techniques is visible at low conductivity intervals from 0 to 250 mS.m^{-1} (Fig. 6a), corresponding to fresh-brackish water conditions ($\text{TDS} < 1500 \text{ mg/L}$, Appendix C). Most ERT-inverted conductivity values (approximately 70%) have a

404 deviation smaller than 30 mS.m^{-1} from what is measured at a higher resolution with EM-log (Fig.
 1 405 6a). This good correspondence is for example observed in LK07-BT and the shallower location (<
 2
 3 406 20 m) in LK01-BT. The ERT values correctly image the gradual increase in conductivity from 150
 4
 5
 6 407 mS.m^{-1} in LK07-BT and 80 mS.m^{-1} in LK01-BT at the depth of 8 m to higher conductivity at larger
 7
 8 408 depths (Fig. 7a and b), corresponding with what is expected in theory for clay-dominated
 9
 10
 11 409 sediments. This reveals the conductive response being governed by lithology.

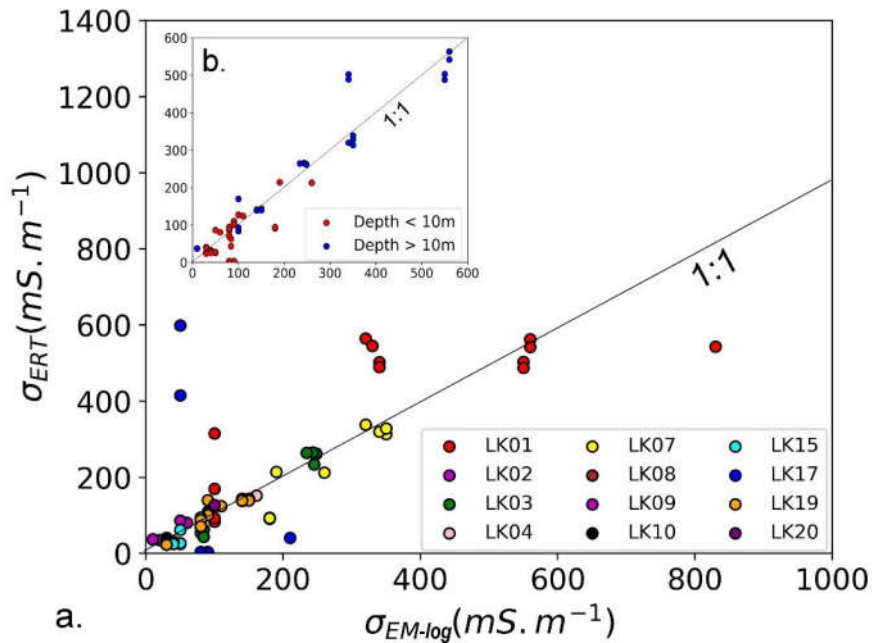


Figure 6. a. Relationship between EM-logs and ERT dataset. The 1:1 lines represent perfect correlations. b. Correlation between EM-log and ERT with depth. The depth division is chosen as 10m based on the averaged mid-depth point of each profile.

410 Nearly 20% of the total investigated points have a difference of $30 - 100 \text{ mS.m}^{-1}$. Such
 411 difference is for example observed between 4 m and 6 m deep in LK03-BT (Fig.7b), where a
 412 decrease in conductivity is shown from 85 mS.m^{-1} to 40 mS.m^{-1} , relatively consistent with the
 413 transition to a coarser category containing a majority of sands and a minority of clay and grit (<
 414 15%) in the lithologs. In contrast to EM-logs at this deep interval, the observed ERT values are
 415 only varying in a limited range from 45 mS.m^{-1} to 65 mS.m^{-1} . This discrepancy could be related to
 416 the limited resolution of the inversions.

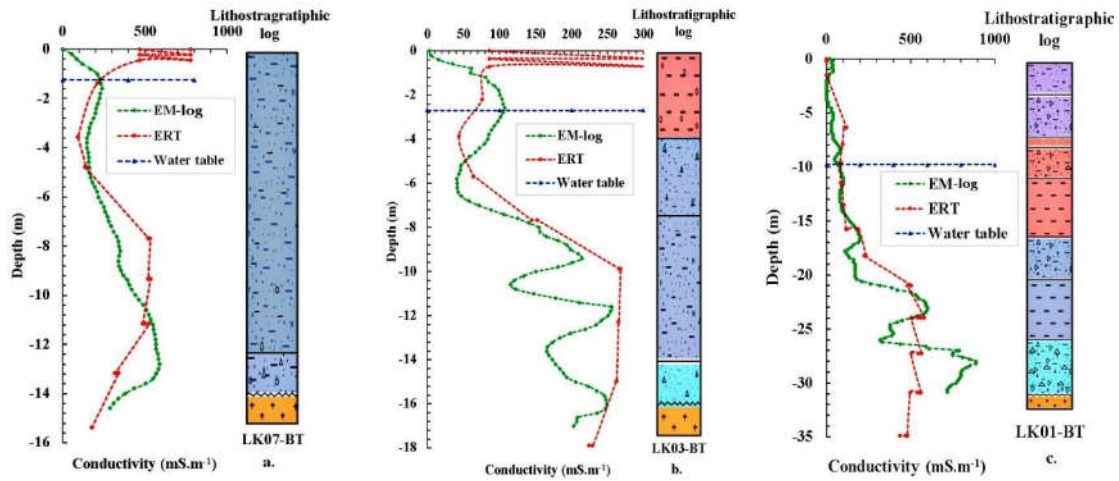


Figure 7. Conductive relationship between EM-logs and ERT dataset.

The tendency of increase in conductivity downward to the bedrock, due to increased salinity in groundwater (Fig. 7), is observed in most EM-logs. However, this trend is not always consistent in inverted models, leading to high differences exceeding 100 mS.m^{-1} . A typical example is for the unconsolidated layers lying on granite bedrock, in LK01-BT (Fig. 7c), the increase in conductivity of EM-log reaches 900 mS.m^{-1} in the gravel layer while that of ERT is much lower (around 500 mS.m^{-1}) and varies insignificantly below the depth of 20 m. The high deviations for these data are caused by the regularization term and loss of the resolution with depth (Day-Lewis et al., 2005; Hermans and Irving, 2017), and sometimes to compensation artefacts (higher resistivity spike causing lower resistivity values below, see for example the obvious outlier in LK07-BT). These effects prevent ERT to provide an as detailed description as combined EM/lithologic logs. However, there is no clear indication that the depth can explain strongly deviating points (Fig. 6b). This implies that a diminishing depth resolution is not the only cause for deviations, but other causing factors such as the presence of inversion artefacts caused by anthropic structures at the surface, the averaging calculation methodology, and the measuring scale play a role. High deviations are also observed near the surface, at depths shallower than 1 m, conductive features in the ERT data fluctuate repeatedly from 80 mS.m^{-1} to 300 mS.m^{-1} in LK03-PT and from 450 mS.m^{-1} to 800 mS.m^{-1} in LK07-BT while EM-logs in both boreholes varies slightly under 150 mS.m^{-1} . This could be related to global smoothing regularization and the above-

435 mentioned artefacts of inversion linked to anthropic structures in the vicinity of the wells (Hermans
1 436 and Irving, 2017; von Bülow et al., 2021).

2
3
4 437 Generally, the ERT and EM-log features show relatively identical trends but ERT data is
5
6 438 recorded through a larger scale and with a lowering resolution with depth, causing deviations from
7
8
9 439 EM-log data. For conductivity values under $250 \text{ mS}\cdot\text{m}^{-1}$ corresponding to fresher conditions, the
10
11 440 ERT inverted models reveal a more accurate quantitative estimation of the bulk electrical
12
13
14 441 conductivity. For higher conductivity values, the ERT inversion models are qualitatively correct
15
16 442 and generally sufficient to conclude the resistivity threshold for saline water that has been reached.

19 443 *4.2.3. Correlation between salinity and ERT data*

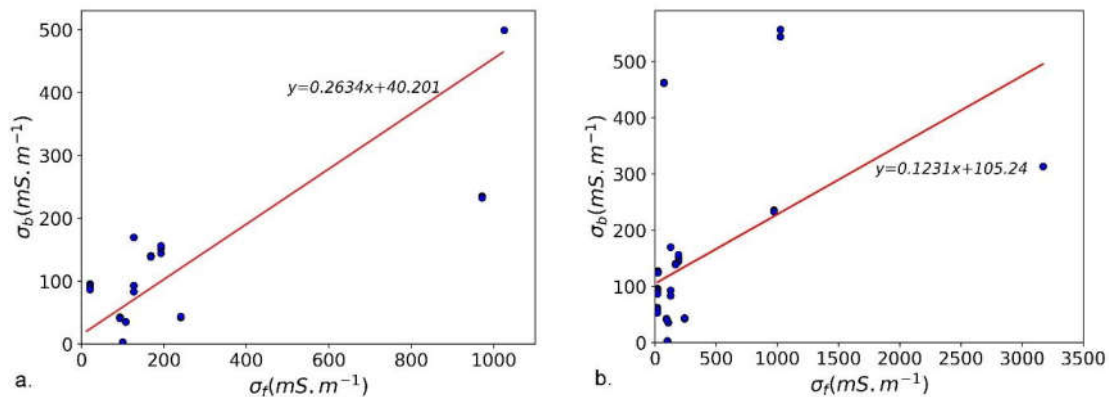
21 444 Figure 8 shows two scatterplots comparing salinity translated into fluid conductivity and
22
23
24 445 bulk conductivity for clay-free and clay-bearing layers. We extracted ERT conductivity values in
25
26 446 boreholes where the water conductivity was measured on groundwater samples. The bulk inverted
27
28
29 447 resistivity at the depth of the screen interval was averaged within a 5 m radius cylinder around the
30
31 448 borehole location.

33 449 Figure 8a represents the sandy sediment. Most points have a water conductivity lower than
34
35
36 450 $250 \text{ mS}\cdot\text{m}^{-1}$, which makes it difficult to derive a strong trend for a broad range of salinities. Most
37
38
39 451 points show a spread around the linear trend line at low conductivity values. Analogously to the
40
41 452 lab methodology, from equation 4, the formation factor and surface conduction can be derived and
42
43 453 are 3.8 and $40.201 \text{ mS}\cdot\text{m}^{-1}$, respectively. The surface conductivity value is larger than in the lab
44
45
46 454 and likely accommodates the averaging nature of resistivity at this scale.

48 455 Figure 8b corresponds to clay-dominated samples. Here, data points are scattered over a
49
50
51 456 wide range of bulk electrical conductivity for a given water conductivity. This scattering is likely
52
53 457 an effect of the variability in the clay content of the various samples, in accordance with what was
54
55
56 458 observed for the surface conduction of laboratory samples, combined with the averaging effect of
57
58 459 ERT. Although deriving a trend is only indicative given the weak tendency, a formation factor of
59
60 460 8.1 and surface conductivity of $105.24 \text{ mS}\cdot\text{m}^{-1}$ are derived.

461 Remarkably, the spread in bulk conductivity observed at the low value of water
 1 462 conductivity is consistent with the expected range observed at the laboratory scale (Fig.3, Table
 2
 3 463 2), spanning almost one order of magnitudes. Similarly, the formation factor values are acceptable
 4
 5 464 for the described lithology and in agreement with lab processing data. However, the field-scale
 6
 7 465 surface conductivity is higher than the lab-scale one. This is likely related to the heterogeneous
 8
 9 466 nature of the sediment sequences in the study area (Fig. 4, 5 and 7). Indeed, the broad grain-sized
 10
 11 467 variation, fraction and dispersion of clay are responsible for deviations from the lab petrophysical
 12
 13 468 relationship.

18 469 The good agreement of ERT with EM-logs at low salinity combined to the large spread
 19
 20 470 observed in the field petrophysical relationship suggests that the clay content has an important
 21
 22 471 impact on the field resistivities. ERT results can therefore be used for qualitative saltwater
 23
 24 472 delineation (high salinity threshold), but should be thoughtfully handled to derive quantitative
 25
 26 473 estimates of the salinity, especially at low salinities, where the clay content dominates the response.



46 Figure 8. Plotting fluid conductivity against bulk conductivity. a. For the clay-free category. b. For the
 47 clay-bearing mixture.
 48
 49

51 474 5. Discussions

52
 53
 54 475 The combination of ERT/TDIP and EM-logs at the field scale with SIP investigations and
 55
 56 476 lithological description at the laboratory scale has allowed us to derive clear threshold values for
 57
 58 477 the interpretation of electrical properties in terms of salinity and heterogeneity.
 59
 60
 61
 62
 63
 64
 65

478 At the small scale, our laboratory data shows that the chargeability is proportional to the
1 479 electrical conductivity of samples and increases with the clay content, except for the maximum
2
3 480 tested clay content (35%), which likely results from sample preparation. This is in accordance with
4
5
6 481 the previous studies, which generally indicate an inverse correlation between increasing
7
8 482 polarization and clay content with decreasing resistivity (Vacquier et al., 1957; Marshall and
9
10 483 Madden, 1959; Ogilvy and Kuzmina, 1972; Klien and Sill, 1982). In other words, the relationship
11
12 484 between the quadrature conductivity and the normalized chargeability is a linear (Viezzoli and
13
14 485 Cull 2005; Revil et al., 2017). A threshold value of 1.5 mS.m^{-1} appears to be a suitable criterion
15
16 486 for discerning the substantial presence of clay minerals. At the field scale, we have observed
17
18 487 relatively low values of normalized chargeability, ranging from approximately 1 mS.m^{-1} to 1.5
19
20 488 mS.m^{-1} , in areas where lithological analysis indicates a low clay content (<15% clay), while
21
22 489 values ranging from 3 to 10 mS.m^{-1} are characteristics of clay layer and lenses (see Fig. 4 and 5).
23
24
25 490 These observations align with the normalized chargeability obtained through the SIP investigation.
26
27
28 491 The analysis of normalized chargeability, when compared with the comprehensive lithological
29
30 492 description and EM-logs, has revealed an intricate distribution pattern of clay minerals
31
32 493 predominantly composed of kaolinite and illite. These minerals exist in various formations within
33
34 494 the subsurface as discontinuous small lenses, occasionally with brackish or saline porewater, or as
35
36 495 more continuous layers with thicknesses ranging from 0.5 m to 5.5 m, acting as regional aquitards
37
38
39 496 (see Fig. 5). Furthermore, clay minerals are frequently dispersed within the sand layers, as
40
41
42 497 illustrated in Figures 4, 5, and 7.
43
44
45
46
47

48 498 Consequently, the use of normalized chargeability assists in distinguishing between clay
49
50 499 content and salinity within the resistivity response. However, depending on field conditions, TDIP
51
52 500 does not always provide good and reliable results. Artefacts and/or data noise can locally distort
53
54 501 inversion results (Slater, 2000; Zarif et al., 2017). Near the surface, the normalized chargeability
55
56 502 is sometimes low, even in the presence of individual clay layers (Fig. 5). The IP data quality
57
58 503 remains a concern, as the signal-to-noise ratio is low, particularly in saline conditions. Not all field
59
60
61
62
63
64
65

504 profiles could be inverted for the (normalized) chargeability because of the suboptimal quality of
1 505 the acquired data. As a consequence, the lack of sufficient co-located samples has impeded the
2
3 506 validation of a definitive relationship between normalized chargeability and clay content at the
4
5
6 507 field scale.

7
8
9 508 The laboratory samples allowed to derive a clear petrophysical relationships for sandy and
10
11 509 clay bearing sediments with consistent formation factors. The surface conductivity is one order of
12
13 510 magnitude larger for the latter, as expected. This approach allowed us to derive threshold values
14
15
16 511 for saline and fresh water for both sediment types (Table 2). The latter appeared to be successful
17
18 512 in delineating saline zones on the field and were also consistent with previous studies (Cong-Thi
19
20
21 513 et al., 2021a).

22
23
24 514 The comparison with lithological and EM-logs at the field scale validated the formation
25
26 515 factor obtained from the SIP investigation, while the field-scale surface conductivity values
27
28 516 appeared higher than the lab-scale ones. The discrepancy could be related to the heterogeneous
29
30
31 517 distribution of sedimentary layers, the coarser-sized aquifers that are alternating with argillaceous
32
33 518 bands/lenses, and the existence of clay minerals dispersed within the pore space, causing an
34
35
36 519 increase of surface conductivity magnitude (Keller and Frischknecht, 1966). Besides, the local
37
38 520 presence of ilmenite (Cong-Thi, 2021b), a conductive mineral, could affect the apparent increase
39
40
41 521 in surface conductivity. Scale and inversion effects, leading to smoothing and averaging in the
42
43 522 resistivity distribution, can also explain the presence of a significant surface conductivity for sand-
44
45
46 523 dominated sediments. In addition, the absence of extremely saline samples at the field scale made
47
48 524 the regression relatively sensitive to a few samples. The spread at low salinities is important,
49
50
51 525 indicating the difficulty to derive field-based petrophysical relationships in highly heterogeneous
52
53 526 coastal aquifers. In the study area, in freshwater conditions ($\sigma_f < 250 \text{ mS.m}^{-1}$, TDS < 1000 mg/L),
54
55
56 527 bulk conductivity seems to be governed by the lithology, and the surface conduction mechanisms
57
58 528 from clay particles dominates over ionic conduction.

529

EM-logs and ERT data generally display similar trends. However, ERT cannot detect thin

1 530

clay sedimentary layers (less than 0.5 m in Fig.7c), due to the poorer vertical resolution. In this

2

3 531

range of salinity, there is a very large spread in the field-based petrophysical relationship,

4

5 532

corresponding to the large heterogeneity observed in the well logs, preventing ERT alone to make

6

7 533

any quantitative interpretation because of the double effect of fluid salinity and clay content. In

8

9 534

saltier conditions generally encountered at larger depths, ERT data still display the same trend as

10

11 535

EM logs. However, ERT cannot systematically discriminate the transition between the complex

12

13 536

sedimentary multi-layers (Fig. 7c) due to its volume-averaging nature of ERT and the loss of

14

15 537

resolution with depth. Nevertheless, ERT seems to be consistent in predicting the salinity threshold

16

17 538

of 9 Ohm.m for saline water (TDS > 3000 mg/L).

18

19

20

21

22

23 539

The electrical response of the bedrock is also well characterized by ERT inverted models

24

25 540

(Fig. 4 and 5), based on resistivity values increasing from about 30 to 100 Ohm.m. These values

26

27 541

are extremely low for what is expected to be unaltered granite (> 1000 Ohm.m) (Lowrie, 2007).

28

29 542

The main contributor to this lower signal is the presence of fracture-filled salty groundwater. The

30

31 543

clay content also increases at the transition between unconsolidated sediments and the lower-lying

32

33 544

bedrock, which is composed of an upper altered granite zone. The weathering stage of the bedrock

34

35 545

seems to vary largely between locations and is superimposed with a possible presence of saltwater

36

37 546

in the bedrock as well. Typically, the unaltered bedrock is identified by an increase in resistivity

38

39 547

and low normalized chargeability, while weathered bedrock is difficult to discriminate from the

40

41 548

above-unconsolidated sediments, as it is characterized by the normalized chargeability varying

42

43 549

from 1.5 mS.m⁻¹ to 3 mS.m⁻¹ and relatively low resistivity. Particularly in the complexity of

44

45 550

predominantly saline conditions, other contributors decreasing the conductivity could be

46

47 551

overshadowed. Here saltwater is the main contributor while clay presence is a co-contributor.

48

49

50

51

52

53

54

55

56

57

58

59

60

61

62

63

64

65

6. Conclusions

59 553

This research systematically investigated the electrical response of heterogeneous clay-

60

61 554

bearing sediments subject to saltwater intrusion processes both in controlled laboratory settings

62

63

64

65

555 and within natural field environments. Threshold values from SIP laboratory measurements for
1 556 both the normalized chargeability and resistivity are combined at the field scale to identify first
2
3 557 clayey sediments from sandy sediments and second apply the appropriate resistivity threshold to
4
5 558 identify fresh from saline porewater. The results are validated with co-located logging data. The
6
7
8 559 information obtained through SIP measurements therefore provides valuable insight into
9
10 560 subsurface heterogeneity that may not be fully resolved through ERT and TDIP data only.
11
12

13
14 561 The findings from both the laboratory and field experiments exhibit a successful alignment
15
16 562 with the established lithological structure as documented in borehole logs and also allow a more
17
18 563 exhaustive interpretation of the lithostratigraphic correlation. As expected, the SIP data contribute
19
20 564 significantly to the characterization of the surface conductivity of clay-containing sedimentary
21
22 565 aggregates.
23
24
25

26 566 The outcomes of our investigation underscore the capability of SIP to discriminate
27
28 567 lithological heterogeneities within unconsolidated sediments, particularly in the presence of clay
29
30 568 minerals. The observed trends in surface conductivity values and formation factors, which increase
31
32 569 from coarser sand to clay-bearing sand, closely adhere to theoretical expectations and closely
33
34 570 resemble the results derived from field interpretations. Nevertheless, it is noteworthy that
35
36 571 petrophysical relationships sourced from field observations exhibit considerable variability around
37
38 572 the established trend, indicating that quantitative estimation is subject to large uncertainty.
39
40
41
42
43

44 573 The trends observed in EM-logs and electrical resistivity tomography (ERT) data within
45
46 574 the field are reasonably consistent. Nevertheless, it is worth noting that the ERT data is recorded
47
48 575 over a larger spatial scale with a lower vertical resolution, causing some deviations compared to
49
50 576 EM-logs. These deviations can be caused by the regularization techniques employed during the
51
52 577 inversion process and the loss of resolution with increasing depth. For sedimentary conditions
53
54 578 characterized by low conductivity values, specifically in falling into fresher conditions under 250
55
56 579 mS.m⁻¹, the ERT model provides a more precise quantitative estimation of the bulk electrical
57
58 580 conductivity and can be used to detect the presence of clay constituents. However, quantitative
59
60
61
62
63
64
65

581 interpretation remains challenging due to the combined effect of salinity and clay content. In such
1 582 cases, the utilization of normalized chargeability proves beneficial in identifying the occurrence
2
3 583 of clay lenses/ layers. For larger conductivity values, the ERT model is able to satisfactorily
4
5 584 identify zones where the salinity exceeds the 3000 mg/L threshold. Nevertheless, it is imperative
6
7
8 585 to emphasize that ERT should not be employed for deriving absolute salinity values in such
9
10
11 586 scenarios.

12
13
14 587 The petrophysical analysis of the data acquired from SIP, ERT, and EM-logs investigations
15
16 588 towards lithology and corresponding salinity pointed out the complexity linked to the very
17
18 589 heterogeneous nature of the study area. Globally, the application of high-resolution ERT/IP
19
20 590 inversions and EM logging has proven to be effective in discriminating the heterogeneity within
21
22
23 591 clay-rich zones, even from saline-contaminated zones. Within clay-rich zones, the bulk electrical
24
25 592 conductivity is amplified due to the concurrent presence of clay minerals and saline water,
26
27
28 593 overshadowing the existence of clay-bearing strata, thereby sometimes mistaken for extreme
29
30
31 594 salinity in the aquifers. Besides, ERT/TDIP data exhibits insensitivity to clay lenses or layers
32
33 595 thinner than 0.5 meters, even at shallow depths. This insensitivity could potentially lead to
34
35 596 misinterpretations, particularly in distinguishing between interbedded sand layers and saline or
36
37
38 597 brackish conditions. In contrast, the ERT model provides a more accurate representation of the
39
40
41 598 electrical response of the underlying bedrock.

42
43 599 **Author Contributions:** D.C.T conceptualized the survey plan, processed the ERT/ IP and SIP
44
45 600 data and applied the methodology, and was responsible for writing the paper. L.P.D contributed to
46
47
48 601 the fieldwork and data processing. D.C contributed to the methodology and SIP processing. X.D.P
49
50
51 602 participated in the ERT/IP processing and EM-log comparison. H.D.T was responsible for sample
52
53 603 preparation and do grain-sized analysis. H.H.H participated in the fieldwork and the
54
55
56 604 conceptualization of the survey plan. N.F. and H.T conceptualized the survey plan and the
57
58 605 methodology and supervised the study.

59
60
61
62
63
64
65

606 **Funding:** This research is funded by The Special Research Fund (BOF), Ghent University
1 607 through the Ph.D. scholarships of the first two authors.
2
3

4 608 **Acknowledgements:** We deeply thank the VIGMR staff for their support on the field and grain-
5
6 609 sized classification. We would like to thank staff members in the laboratory of the Urban &
7
8 610 Environmental Engineering, Liège University, who assisted us in the analysis of SIP
9
10 611 measurements.
11
12
13

14 612 **Conflicts of Interest:** The authors declare no conflict of interest.
15
16
17

18 613 **References**

19
20

- 21 614 1. Alabi, A.A., Ogunbe, A.S., Adebo, B., Lamina, O., 2010. Induced polarization interpretation
22
23 615 for subsurface characterization: A case study of obadore, lagos state. Archives Physics
24
25 616 Research 1, pp. 34–43.
26
27
28
- 29 617 2. Archie, G.E., 1942. The electrical resistivity log as an aid in determining some reservoir
30
31 618 characteristics. Trans AIME 146, pp. 54–62.
32
33
- 34 619 3. ASTM D422-63,. 2007. Standard Test Method for Particle-Size Analysis of Soils, ASTM
35
36 620 International, West Conshohocken, PA.
37
38
39
- 40 621 4. Attwa, M., Günther, T., Grinat, M., Binot, F., 2011. Evaluation of DC, FDEM, and IP
41
42 622 resistivity methods for imaging perched saltwater and a shallow channel within coastal tidal
43
44 623 flat sediments. Journal of Applied Geophysics 75, pp. 656–670.
45
46
47
- 48 624 5. Baines, D., Smith, D.G., Froese, D.G., Bauman, P., Nimeck, G., 2022. Electrical resistivity
49
50 625 ground imaging (ERGI): A new tool for mapping the lithology and geometry of channel-belts
51
52 626 and valley-fills. Sedimentology 49, pp. 441–449.
53
54
- 55 627 6. Benoit, S., Ghysels, G., Gommers, K., Hermans, T., Nguyen, F., Huysmans, M., 2019.
56
57 628 Characterization of spatially variable riverbed hydraulic conductivity using electrical
58
59
60
61
62
63
64
65

- 629 resistivity tomography and induced polarization. *Hydrogeology Journal* 1, pp. 395–407.
1 630 <https://doi.org/10.1007/s10040-018-1862-7>.
- 2
3 631 7. Börner, F.D., Schopper, J.R. and Weller, A., 1996. Evaluation of transport and storage
4
5 632 properties in the soil and groundwater zone from induced polarization measurements.
6
7 633 *Geophysical Prospecting* 44(4), pp. 583–601.
- 8
9
10 634 8. Changa, Yawen., X. Hua Bill., Xu, Zexuan., Lia, Xue., Tong, Juxiu., Chen, Lin., Zhang,
11
12 635 Hanxiong., Miaoe, Jinjie., Liue, Hongwei., Mae, Zhen., 2018. Numerical simulation of
13
14 636 seawater intrusion to coastal aquifers and brine water/freshwater interaction in south coast of
15
16 637 Laizhou Bay, China. *Journal of Contaminant Hydrology*, 215, pp: 1-10.
17
18 638 <https://doi.org/10.1016/j.jconhyd.2018.06.002>.
- 19
20
21 639 9. Cole, K. S., and R. H. Cole., 1941. Dispersion and absorption in dielectrics. I. Alternating
22
23 640 current characteristics, *The Journal of Chemical Physics* 9, pp. 341–351.
- 24
25
26 641 10. Cong-Thi, D., Dieu, L.P., Thibaut, R., Paepen, M., Huu, H.H., Nguyen, F., Hermans, T.,
27
28 642 2021a. Imaging the structure and the saltwater intrusion extent of the Luy River coastal aquifer
29
30 643 (Binh Thuan, Vietnam) using electrical resistivity tomography. *Water* 2021 13, 1743 pp.
31
32 644 <https://doi.org/10.3390/w13131743>.
- 33
34
35 645 11. Cong-Thi, D., Pham Dieu, L., Huu Hieu, H., Nguyen, F., Hermans, T., 2021b. Granulometric
36
37 646 and lithological composition of sediment in the boreholes along the Luy river in Bac Binh
38
39 647 discs., Binh Thuan province: results and interpretation. Report. Ghent University, Belgium.
40
41 648 Unpublished.
- 42
43
44 649 12. Dahlin, T., Leroux, V., & Nissen, J., 2002. Measuring techniques in induced polarisation
45
46 650 imaging. *Journal of Applied Geophysics* 50, pp. 279–298.
- 47
48
49 651 13. Dahlin, T., and Leroux, V., 2012. Improvement in time-domain induced polarization data
50
51 652 quality with multi-electrode systems by separating current and potential cables. *Near Surface*
52
53 653 *Geophysics* 10, 1957 pp. <https://doi.org/10.3997/1873-0604.2012028>.
- 54
55
56
57
58
59
60
61
62
63
64
65

- 654 14. Dieu, L.P., Cong-Thi, D., Segers, T., Huu, H.H., Nguyen, F., Hermans, T., 2022. Groundwater
1 655 Salinization and Freshening Processes in the Luy River Coastal Aquifer, Vietnam. *Water* 14
2
3 656 (15), 2358 pp.
4
5
6 657 15. Dickinson, W.R and Suczek, C.A., 1979. Plate tectonics and sandstone compositions.
7
8 658 *American Association of Petroleum Geologist* 63, pp. 2164–2182.
9
10
11 659 16. Dukhin S.S. and Shilov P., 1974. Dielectric Phenomena and the Double Layer in Disperse
12
13 660 Systems and Polyelectrolytes. John Wiley & Sons, Inc., New York.
14
15
16 661 17. Evrard, M., Dumont, G., Hermans, T., Chouteau, M., Francis, O., Pirard, E., Nguyen, F., 2018.
17
18 662 Geophysical Investigation of the Pb–Zn Deposit of Lontzen–Poppelsberg, Belgium. *Minerals*
19
20 663 8, 233 pp. <https://doi.org/10.3390/min8060233>.
21
22
23 664 18. Everett, M.E., 1997. Transient inductive coupling of loops over near-surface clay-bearing
24
25 665 sandstones. *Society of Exploration Geophysicists 67th Ann. Internat. Mtg.* (Dallas, TX,
26
27 666 November 2-7).
28
29
30 667 19. Hayashi, M., 2004. Temperature-electrical conductivity relation of water for environmental
31
32 668 monitoring and geophysical data inversion. *Environment Monitoring Assessment* 96, pp. 119–
33
34 669 128.
35
36
37 670 20. Hermans, T., Nguyen, F., Robert, T., Revil, A., 2014. Geophysical methods for monitoring
38
39 671 temperature changes in shallow low enthalpy geothermal systems. *Energies* 7, pp. 5083–5118.
40
41
42 672 21. Hermans, T., Wildemeersch, S., Jamin, P., Orban, P., Brouyère, S., Dassargues, A., Nguyen,
43
44 673 F., 2015. Quantitative temperature monitoring of a heat tracing experiment using cross-
45
46 674 borehole ERT. *Geothermics* 53, pp. 14–26.
47
48
49
50 675 22. Hoang, P., 1997. Geological and Mineral Map of Phan Thiet, scale 1:50.000. *Cent. Inf. Arch.*
51
52 676 *J. Geol.* C-49-37-A. Accessed on: [http://idm.gov.vn/1P1NPIT/vi-VN/Ban-Do-Dia-](http://idm.gov.vn/1P1NPIT/vi-VN/Ban-Do-Dia-Chat.aspx)
53
54 677 [Chat.aspx](http://idm.gov.vn/1P1NPIT/vi-VN/Ban-Do-Dia-Chat.aspx). (In Vietnamese). Accessed available: [http://idm.gov.vn/1P1NPIT/vi-VN/Ban-Do-](http://idm.gov.vn/1P1NPIT/vi-VN/Ban-Do-Dia-Chat.aspx)
55
56 678 [Dia-Chat.aspx](http://idm.gov.vn/1P1NPIT/vi-VN/Ban-Do-Dia-Chat.aspx). (In Vietnamese).
57
58
59
60
61
62
63
64
65

- 679 23. Hördt, A., et al., 2016. The dependence of induced polarization on fluid salinity and pH,
1 680 studied with an extended model of membrane polarization. *J. Applied Geophysics* 135, pp.
2
3 681 408–417. <http://dx.doi.org/10.1016/j.jappgeo.2016.02.007>.
4
5
6 682 24. Hördt, A., Bairlein, K., Bückner, M., Stebner, H., 2017. Geometrical constraints for membrane
7
8 683 polarization. *Near Surface Geophysics* 15 (6), pp. 579–592. [https://doi.org/10.3997/1873-](https://doi.org/10.3997/1873-0604.2017053)
9
10 684 0604.2017053.
11
12
13 685 25. Hort, Ryan D., Revil, André., Munakata-Marr, Junko., 2014. Analysis of sources of bulk
14
15 686 conductivity change in saturated silica sand after unbuffered TCE oxidation by permanganate.
16
17
18 687 *Journal of Contaminant Hydrology*, 165, pp 11-23.
19
20 688 <https://doi.org/10.1016/j.jconhyd.2014.07.003>.
21
22
23 689 26. Huisman, J.A., Zimmermann, E., Esser, O., Haegel, F.-H., Treichel, A., Vereecken, H., 2016.
24
25 690 Evaluation of a novel correction procedure to remove electrode impedance effects from
26
27
28 691 broadband SIP measurements. *Journal of Applied Geophysics*. [http://doi.org/10.1016/](http://doi.org/10.1016/j.jappgeo.2015.11.008)
29
30 692 [j.jappgeo.2015.11.008](http://doi.org/10.1016/j.jappgeo.2015.11.008).
31
32
33 693 27. Keller, G.V., Frischknecht, F.C., 1966. *Electrical Methods in Geophysical Prospecting*;
34
35 694 Pergamon Press: Oxford, UK.
36
37
38 695 28. Kemna, A., Binley, A., Cassiani, G., Niederleithinger, E., Revil, A., Slater, L., Williams,
39
40 696 K.H., Orozco1, A.F., Haege, F.H., Hördt, A., Kruschwitz, S., Leroux, V., Titov, K., and
41
42 697 Zimmermann, E., 2012. An overview of the spectral induced polarization method for near-
43
44
45 698 surface applications. *Near Surface Geophysics* 10, pp. 453-468. [http://doi:10.3997/1873-](http://doi:10.3997/1873-0604.2012027)
46
47 699 0604.2012027.
48
49
50 700 29. Kemna, A., 2000. *Tomographic Inversion of Complex Resistivity-Theory and Application*.
51
52 701 Ph.D. Thesis. Ruhr Universität, Bochum, Germany.
53
54
55 702 30. Ketabchi, Hamed., Sina Jahangir, Mohammad., 2021. Influence of aquifer heterogeneity on
56
57 703 sea level rise-induced seawater intrusion: A probabilistic approach. *Journal of Contaminant*
58
59 704 *Hydrology*, 236, 103753.
60
61
62 705 31. <https://doi.org/10.1016/j.jconhyd.2020.103753>
63
64
65

- 706 32. Klien, J. D., and Sill, W. R., 1982. Electrical properties of artificial claybearing sandstone:
1 707 Geophysics 47, pp. 1593–1605.
2
- 3 708 33. Korošak, Dean., Cvikl, Bruno., Kramer, Janja., Jecl, Renata., Prapotnik, Anita., 2007.
4
5 709 Fractional calculus applied to the analysis of spectral electrical conductivity of clay–water
6
7 710 system. Journal of Contaminant Hydrology, 92, pp 1-9.
8
9 711 <https://doi.org/10.1016/j.jconhyd.2006.11.005>.
10
- 11 712 34. Kremer, Thomas., Schmutz, Myriam., Leroy, Philippe., Agrinier, Pierre., Mainault, Alexis.,
12
13 713 2016. Modelling the spectral induced polarization response of water-saturated sands in the
14
15 714 intermediate frequency range (102–105 Hz) using mechanistic and empirical approaches.
16
17 715 Geophysical Journal International, 207, 2, pp 1303–1312. <https://doi.org/10.1093/gji/ggw334>.
18
19 716 35. Krumbein, W.C., 1934. Size frequency distribution of sediments: Journal of Sedimentary
20
21 717 Petrology 4,pp. 65-77.
22
- 23 718 36. Krumbein, W. C., and Sloss, L. L., 1963. Stratigraphy and sedimentation: 2nd ed., W. H.
24
25 719 Freeman, San Francisco, 660 pp.
26
- 27 720 37. Leroy, P., Revil, A., Kemna, A., Cosenza, P., Ghorbani, A., 2008. Complex conductivity of
28
29 721 water-saturated packs of glass beads. Journal of Colloid Interface Science 321 (1), pp. 103–
30
31 722 117. <https://doi.org/10.1016/j.jcis.2007.12.031>.
32
- 33 723 38. Lesmes, D.P. and Morgan F.D., 2001. Dielectric spectroscopy of sedimentary rocks. Journal
34
35 724 of Geophysical Research 106, pp. 13329–13346.
36
- 37 725 39. de Lima O.A.L. and Sharma M.M., 1992. A generalized Maxwell-Wagner theory for
38
39 726 membrane polarization in shaly sands. Geophysics 57(3), pp. 431–440.
40
- 41 727 40. L. Insigne, M.S., and Kim, G.S., 2010. Saltwater Intrusion Modeling in the Aquifer Bounded
42
43 728 by Manila Bay and Parañaque River, Philippines. Environmental Engineering Research 15
44
45 729 (2), pp. 117-121. <http://doi.10.4491/eer.2010.15.2.117>. pISSN 1225-1025 eISSN 2005-968X.
46
47 730 41. Loke, M.H., 2011. Tutorial: 2-D and 3-D Electrical Imaging Surveys.
48
- 49 731 42. Loke, M. H., Barker, R. D., 1996. Rapid least squares inversion of apparent resistivity
50
51 732 pseudosections by a quasi-Newton method. Geophysical Prospecting 44, pp. 131-152.
52
53
54
55
56
57
58
59
60
61
62
63
64
65

- 733 43. Lowrie, W., 2007. Fundamentals of Geophysics, second edition. Assessed available:
1 734 <http://ebooks.cambridge.org/ebook.jsf?bid=CBO9780511807107>.
2
- 3 735 44. Magnusson, M., Fernlund, J.R., Dahlin, T., 2010. Geoelectrical imaging in the interpretation
4
5
6 736 of geological conditions affecting quarry operations. Bull. Engineering Geology Environment
7
8 737 69, pp. 465–486.
9
- 10 738 45. Martínez, J., Benavente, J., García-Aróstegui, J.L., Hidalgo, M.C., Rey, J., 2009. Contribution
11
12
13 739 of electrical resistivity tomography to the study of detrital aquifers affected by seawater
14
15 740 intrusion–extrusion effects: The river Vélez Delta (Vélez-Málaga, Southern Spain).
16
17
18 741 Engineering Geology 108, pp. 161–168.
19
- 20 742 46. Marshall, D. J., and Madden, T. R., 1959. Induced polarization, a study of its causes:
21
22
23 743 Geophysics 24, pp. 790–816.
24
- 25 744 47. McNeill, J.D., Bosnar, M., and Snelgrove, F.B., 1990. Resolution of an electromagnetic
26
27
28 745 borehole conductivity logger for geotechnical and ground water applications: Geonics
29
30 746 Technical Note TN–25, 28 pp.
31
- 32 747 48. Merriam J.B., 2007. Induced polarization and surface electrochemistry. Geophysics 72 (4),
33
34
35 748 pp. 157-166.
36
37
- 38 749 49. Miall, A.D., 2000. Principles of Sedimentary Basin Analysis. Third, updated and enlarged
39
40 750 edition. ISBN 978-3-642-08506-2. ISBN 978-3-662-03999-1 (eBook). <https://doi>
41
42
43 751 [10.1007/978-3-662-03999-1](https://doi.org/10.1007/978-3-662-03999-1).
44
- 45 752 50. Michael, HA., Scott, K.C., Koneshloo, M., Yu, X., Khan, M.R., Li, L., 2016. Geologic
46
47
48 753 influence on groundwater salinity drives large seawater circulation through the continental
49
50
51 754 shelf. Geophysical Research Letters 43, pp. 10782–10791.
52
53 755 <https://doi.org/10.1002/2016GL070863>.
54
55
- 56 756 51. Moraa, Abrahan., Mahlknecht, Jürgen., Ledesma-Ruizb, Rogelio., E. Sanfordc., William.,
57
58 757 E. Lesser, Luis,. 2020.Dynamics of major and trace elements during seawater intrusion in a
59
60
61
62
63
64
65

- 758 coastal sedimentary aquifer impacted by anthropogenic activities. *Journal of Contaminant*
1 759 *Hydrology*, 232, pp 103653. <https://doi.org/10.1016/j.jconhyd.2020.103653>.
2
3
- 4 760 52. Motallebiana, Mahdi., Ahmadi, Hojjat., Raoof, Amir., Cartwright, Nick., 2019. An
5
6 761 alternative approach to control saltwater intrusion in coastal aquifers using a freshwater
7
8 762 surface recharge canal. *Journal of Contaminant Hydrology*, 222, pp.56-64.
9
10 <https://doi.org/10.1016/j.jconhyd.2019.02.007>.
11 763
12
13
- 14 764 53. Najib, Saliha., Fadili, Ahmed., Mehdi, Khalid., Riss, Joëlle., Makan, Abdelhadi., 2017.
15
16 765 Contribution of hydrochemical and geoelectrical approaches to investigate salinization
17
18 766 process and seawater intrusion in the coastal aquifers of Chaouia, Morocco. *Journal of*
19
20 *Contaminant Hydrology*, 198, pp.24-36. <http://dx.doi.org/10.1016/j.jconhyd.2017.01.003>.
21 767
22
23
- 24 768 54. Nasiri, Mina., Moghaddam, Hamid Kardan., Hamidi, Mehdi., 2021.. Development of Multi-
25
26 769 Criteria Decision Making Methods for Reduction of Seawater Intrusion in Coastal Aquifers
27
28 Using SEAWAT Code. *Journal of Contaminant Hydrology*, 242, 103848.
29 770
30 <https://doi.org/10.1016/j.jconhyd.2021.103848>
31 771
32
33
- 34 772 55. Ntarlagiannis, D., Williams, K.H., Slater, L., Hubbard, S., 2005a. Low-frequency electrical
35
36 773 response to microbial induced sulfide precipitation. *Journal of Geophysical. Research* 110.
37
38 G02009. <https://doi.org/10.1029/2005JG000024>.
39 774
40
41
- 42 775 56. Nguyen, F., Kemna, A., Antonsson, A., Engesgaard, P., Kuras, O., Ogilvy, R., Gisbert, J.,
43
44 776 Jorreto, S., and Pulido-Bosch, A., 2009. Characterization of seawater intrusion using 2D
45
46 777 electrical imaging. *Near Surface Geophysics* 7, No. 5–6: pp. 377–390.
47
48
49
- 50 778 57. Nguyen, T.T., Karl, S., Danie, U., Charles, N., Phung, V.P., Paul, L., DeMaster, D., Bui,
51
52 779 V.D., Le, D.A., Mai, D.D., 2017. Surface sediment grain-sized distribution and sediment
53
54 780 transport in the subaqueous Mekong Delta, Vietnam. *Vietnam Journal of Earth Sciences*
55
56 781 39(3), pp. 193-209, DOI: 10.15625/0866-7187/39/3/10266. Assessed available:
57
58 <https://vjs.ac.vn/index.php/jse/article/view/10266/pdf>.
59 782
60
61
62
63
64
65

- 783 58. Nguyen Van Vuong., 1991. The quantitative lithological method for recognition of the
1 784 unconsolidated sedimentary formation environments. *Journals of geology*, pp. 206 – 207.
2
3 785 Assessed available: http://www.idm.gov.vn/nguon_luc/Xuat_ban/1991/a20611.htm.(In
4
5
6 786 Vietnamese)
- 7
8 787 59. Ogilvy, A. A., and Kuzmina, E. N., 1972. Hydrogeologic and engineering-geologic
9
10 788 possibilities for employing the method of induced potentials: *Geophysics* 37, pp. 839–861.
11
12 789 60. Olhoeft, G. R., 1985. Low-frequency electrical properties, *Geophysics* 50, pp. 2492–2503.
13
14 790 61. Post, V.E.A., M. Eichholz, R. Brentführer., 2018. Groundwater management in coastal zones.
15
16 791 Bundesanstalt für Geowissenschaften und Rohstoffe (BGR). Hannover, Germany, 107 pp.
17
18 792 Assessed available:
19
20 793 [https://www.bgr.bund.de/EN/Themen/Wasser/Produkte/Downloads/groundwater_managem](https://www.bgr.bund.de/EN/Themen/Wasser/Produkte/Downloads/groundwater_management_in_coastal_zones.pdf?__blob=publicationFile&v=3)
21
22 794 [ent_in_coastal_zones.pdf?__blob=publicationFile&v=3](https://www.bgr.bund.de/EN/Themen/Wasser/Produkte/Downloads/groundwater_management_in_coastal_zones.pdf?__blob=publicationFile&v=3).
23
24 795 62. Revil, A., Coperey A., Shao, Z., Florsch, N., Fabricius, I. L., Deng, Y., Delsman, J. R., Pauw,
25
26 796 P. S., Karaoulis, M., De Louw, P. G. B., Van Baaren, E. S., Dabekaussen, W., Menkovic, A.,
27
28 797 and Gunnink, J. L ., 2017. Complex conductivity of soils, *Water Resource Research* 53, pp.
29
30 798 7121–7147, doi:10.1002/ 2017WR020655.
31
32 799 63. Revil A., 2012. Spectral induced polarization of shaly sands: Influence of the electrical double
33
34 800 layer. *Water Resources Research* 48(2), W02517, doi:10.1029/2011WR011260.
35
36 801 64. Revil, A., and M. Skold., 2011. Salinity dependence of spectral induced polarization in sands
37
38 802 and sandstones, *Geophysical Journal International* 187, pp. 813–824, doi:10.1111/j.1365-
39
40 803 246X.2011.05181. x.
41
42 804 65. Revil, A. & Florsch, N., 2010. Determination of permeability from spectral induced
43
44 805 polarization data in granular media, *Geophysical Journal International* 181, pp. 1480–1498,
45
46 806 doi:10.1111/j.1365-246X.2010.04573.x
47
48
49 807 66. Ronald L. Malcolm and V. C. Kennedy., 1970. Variation of Cation Exchange Capacity and
50
51 808 Rate with Particle Size in Stream Sediment. *Journal (Water Pollution Control Federation)*,
52
53
54
55
56
57
58
59
60
61
62
63
64
65

809 Vol. 42, No. 5, Research Supplement to: 42, 5, Part II pp. 153-160.

1 810 <https://www.jstor.org/stable/25036587>.

2
3
4 811 67. Saneiyani, S., Ntarlagiannis, D., Werkema, D.D., Ustra, A., 2018. Geophysical methods for

5
6 812 monitoring soil stabilization processes. *Journal of Applied Geophysics* 148, pp. 234–244.

7
8
9 813 <https://doi.org/10.1016/j.jappgeo.2017.12.008>.

10
11 814 68. Sara, J., Anders, L., Gianluca, F., and Dahlin, T., 2020. Spectral induced polarization of

12
13 815 limestones: time domain field data, frequency domain laboratory data and physicochemical

14
15 816 rock properties. *Geophysical Journal International* 220, pp. 928–950. <https://doi:>

17
18 817 [10.1093/gji/ggz504](https://doi.org/10.1093/gji/ggz504).

19
20
21 818 69. Slater, L.D., Lesmes, D., 2002. IP interpretation in environmental investigations. *Geophysics*.

22
23 819 67, pp. 77–88.

24
25 820 70. Slater, L., Binley, A., Daily, W., Johnson, R., and Binley, A., 2000. Cross-hole electrical

26
27 821 imaging of a controlled saline tracer injection: *Journal of Applied Geophysics* 44, pp. 85–

28
29 822 102.

30
31
32
33 823 71. Szalai, S., Novák, A., Szarka, L., 2009. Depth of investigation and vertical resolution of

34
35 824 surface geoelectric arrays. *Journal of Environmental and Engineering Geophysics* 14(1),

36
37 825 pp.15–23. <https://doi.org/10.2113/JEEG14.1.15>.

38
39
40 826 72. Ta T.K.O., Nguyen V.L., Kobayashi I., Tateishi M and Saito Y., 2001. Late Pleistocene-

41
42 827 Holocene stratigraphy and delta progradation, the Mekong River delta, South Vietnam.

43
44 828 *Gondwana Research* 4(4), 779 pp. Assessed available:

45
46 829 [https://www.academia.edu/56550912/Late_Pleistocene_Holocene_Stratigraphy_and_Delta_](https://www.academia.edu/56550912/Late_Pleistocene_Holocene_Stratigraphy_and_Delta_Progradation_the_Mekong_River_Delta_South_Vietnam)

47
48 830 [Progradation_the_Mekong_River_Delta_South_Vietnam](https://www.academia.edu/56550912/Late_Pleistocene_Holocene_Stratigraphy_and_Delta_Progradation_the_Mekong_River_Delta_South_Vietnam).

49
50
51
52 831 73. Tarasov, A., and Titov, K., 2007. Relaxation time distribution from time domain induced

53
54 832 polarization measurements, *Geophysical Journal International* 170, pp. 31–43.

55
56
57 833 74. Tassy, A., Maxwell, M., Borgomano, J., Arfib, B., Fournier, F., Gilli, E., and Guglielmi, Y.,

58
59 834 2014. Electrical resistivity tomography (ERT) of a coastal carbonate aquifer (Port-Miou, SE

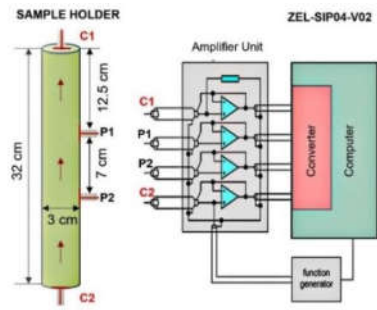
60
61
62
63
64
65

- 835 France). *Environmental Earth Sciences* 71, pp. 601–608. [http://doi.10.1007/s12665-013-](http://doi.10.1007/s12665-013-2802-4)
1 836 2802-4.
2
3 837 75. Titov, K., Tarasov, A., Ilyin, Y., Seleznev, N., Boyd, A., 2010. Relationships between induced
4
5 838 polarization relaxation time and hydraulic properties of sandstone. *Geophysical Journal*
6
7 839 *International* 180, pp. 1095–1106. <https://doi.org/10.1111/j.1365-246X.2009.04465.x>.
8
9
10 840 76. Titov, K., Kemna, A., Tarasov, A., and Vereecken, H., 2004. Induced Polarization of
11
12 841 Unsaturated Sands Determined through Time Domain Measurements. *Vadose Zone Journal*
13
14 842 Vol 3, pp. 1160–1168.
15
16
17 843 77. Tran, N., Nguyen-Thanh, L., Dinh, X.T., Pham, N.H.V., Nguyen, H.S., Tran, T.T.N., 2007.
18
19 844 Quaternary sedimentary cycles in relation to sea level change in Vietnam. *VNU Journal of*
20
21 845 *Science, Earth Sciences* 23, pp. 235-243.
22
23
24 846 78. Vacquier, V., Holmes, R., Kintzinger, P. R., and Lavergne, M., 1957. Prospecting for ground
25
26 847 water by induced electrical polarization: *Geophysics* 22, pp. 660–687.
27
28
29 848 79. Vandenbohede, A., Lebbe, L., Gysens, S. & De Wolf, P., 2008. Infiltration of salt water in
30
31 849 artificial sea inlets in the Belgian dune area. In: *Proceedings of the 1st SWIM-SWICA (19th*
32
33 850 *Salt Intrusion Meeting – 3 rd Salt Water Intrusion in Coastal Aquifers)*, pp. 239- 245.
34
35
36 851 80. Vaudelet, P., Revil, A., Schmutz, M., Franceschi, M. and Bégassat, P., 2011. Induced
37
38 852 polarization signatures of cations exhibiting differential sorption behaviors in saturated sands.
39
40 853 *Water Resources Research* 47(2), W02526, doi:10.1029/2010WR009310.
41
42
43 854 81. Vinegar, H.J. and Waxman, M.H., 1984. Induced Polarization of Shaly Sands. *Geophysics* 49,
44
45 855 pp. 1267-1287. <http://dx.doi.org/10.1190/1.1441755>.
46
47
48 856 82. von Bülow, R., Klitzsch, N., and Wellmann, F., 2021. Strategies to overcome near surface
49
50 857 disturbances while inverting time-lapse surface ERT data. *Journal of Applied Geophysics*
51
52 858 195,104463 pp. <https://doi.org/10.1016/j.jappgeo.2021.104463>.
53
54
55 859 83. Waxman, W.H., Smits L.J.M., 1968. Electrical conductivities in oil-bearing sands. *Social*
56
57 860 *Petroleum Engineering Journal* 8, pp. 107-122.
58
59
60
61
62
63
64
65

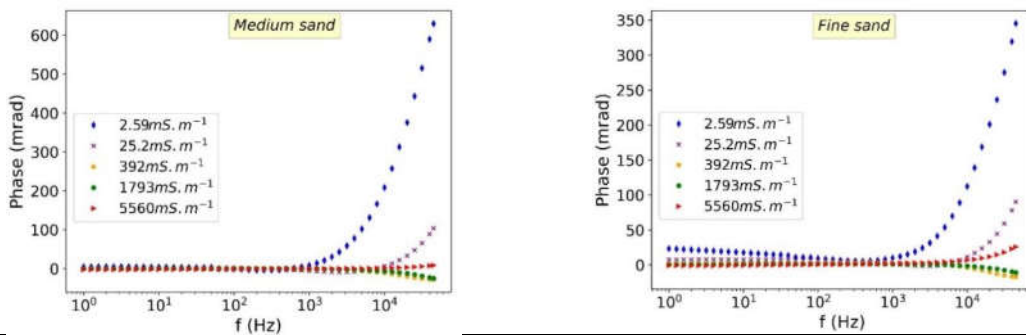
- 861 84. Weigand, M., and Kemna, A., 2016. Relationship between Cole-Cole model parameters and
1 862 spectral decomposition parameters derived from SIP data. *Geophysical Journal International*
2
3 863 205, pp. 1414–1419. <https://doi: 10.1093/gji/ggw099>.
4
5
6 864 85. Werner, Adrian D., Bakker , Mark,. Post, Vincent E.A,. Vandenbohede, Alexander., Lu,
7
8 865 Chunhui., Ataie-Ashtiani, Behzad., Simmons, Craig T., Barry , D.A., 2013. Seawater intrusion
9
10 866 processes, investigation and management: Recent advances and future challenges. *Advance*
11
12 867 *in Water Resources*, 51, pp 3-26. <https://doi.org/10.1016/j.advwatres.2012.03.004>
13
14
15
16 868 86. Wentworth, C. K., 1922. A scale of grade and class terms for clastic sediments. *Journal of*
17
18 869 *Geology*, vol. 30, 377 pp.
19
20
21 870 87. Zimmermann, E., Kemna, A., Berwix, J., Glaas, W., Münch, H.M., Huismann, J.A., 2008. A
22
23 871 high-accuracy impedance spectrometer for measuring sediments with low polarizability.
24
25 872 *Measurement Science and Technology* 19, 105603 pp. doi:10.1088/0957-0233/19/10/105603.
26
27
28
29 873 88. Zarif, F., Kessouri, P., and Slater, L., 2017. Recommendations for field-scale induced
30
31 874 polarization (IP) data acquisition and interpretation. *Journal of Environmental and*
32
33 875 *Engineering Geophysics*. Volume 22, Issue 4, pp. 395–410. <http://doi.10.2113/JEEG22.4.395>.
34
35
36
37 876 89. Zimmermann, E., Huisman, J.A., Kemna, A., Berwix, J., Glaas, W., Meier, H., Wolters, B.,
38
39 877 Esser, O., 2010. Advanced electrical impedance tomography system with high phase
40
41 878 accuracy. Presented at the 6th World Congress on Industrial Process Tomography, pp. 583–
42
43
44 879 591.
45
46
47

880 APPENDIX

- 881 A. SIP measurements (Zimmermann et al., 2008) and our cylinder-shaped sample holder.
51
52
53
54
55
56
57
58
59
60
61
62
63
64
65



882 **B.:** Normalized chargeability of the clay-bearing groups is calculated in the frequency domain. Graphs
 883 refer to phase shift spectra through the five salinity solutions in medium and fine sand categories are nearly
 884 flat at the low-frequency range.



Clay content (%)	Fz	Quadrature conductivity (mS.m ⁻¹)					Normalized chargeability (mS.m ⁻¹)				
		2.59 mS.m ⁻¹	25.2 mS.m ⁻¹	392 mS.m ⁻¹	1793 mS.m ⁻¹	5560 mS.m ⁻¹	2.59 mS.m ⁻¹	25.2 mS.m ⁻¹	392 mS.m ⁻¹	1793 mS.m ⁻¹	5560 mS.m ⁻¹
17	1.00E+03	0.6793	0.6642	1.2029	1.6826	2.1245	3.4	3.3	6.0	8.4	10.6
	1.00E+02	0.3507	0.3548	0.6957	0.9954	1.2828	1.8	1.8	3.5	5.0	6.4
	1.00E+01	0.1933	0.1727	0.4395	0.5580	0.7482	1.0	0.9	2.2	2.8	3.7
	1.00E+00	0.1082	0.1009	0.2721	0.1836	0.1856	0.5	0.5	1.4	0.9	0.9
25	1.00E+03	1.5489	1.4770	1.5673	1.5311	1.3702	7.7	7.4	7.8	7.7	6.9
	1.00E+02	0.8694	0.8514	0.9355	0.9366	0.8488	4.3	4.3	4.7	4.7	4.2
	1.00E+01	0.5385	0.4739	0.5398	0.4349	0.1389	2.7	2.4	2.7	2.2	0.7
	1.00E+00	0.3140	0.2630	0.2958	0.2167	0.2343	1.6	1.3	1.5	1.1	1.2
30	1.00E+03	1.8086	1.8580	1.7468	1.8274	2.0637	9.0	9.3	8.7	9.1	10.3
	1.00E+02	1.0870	1.1444	1.0723	1.1911	1.1563	5.4	5.7	5.4	6.0	5.8
	1.00E+01	0.6172	0.6503	0.5907	0.5868	0.3364	3.1	3.3	3.0	2.9	1.7
	1.00E+00	0.3013	0.3365	0.2672	0.2591	0.2106	1.5	1.7	1.3	1.3	1.1
35	1.00E+03	1.2522	1.1349	1.7622	2.0788	2.9548	6.3	5.7	8.8	10.4	14.8
	1.00E+02	0.6195	0.5688	0.8976	1.0685	1.5365	3.1	2.8	4.5	5.3	7.7
	1.00E+01	0.3324	0.3176	0.4127	0.3596	0.4324	1.7	1.6	2.1	1.8	2.2
	1.00E+00	0.1733	0.1723	0.1743	0.0488	0.3175	0.9	0.9	0.9	0.2	1.6

885 **C.** Total dissolved content (TDS) and electrical conductivity in the drilled boreholes of the Luy River
 886 Catchment in both dry and rainy seasons during two years.

Boreholes			2020	2021	
No	Name	Depth (m)	Rainy season	Dry season	Rainy season

1
2
3
4
5
6
7
8
9
10
11
12
13
14
15
16
17
18
19
20
21
22
23
24
25
26
27
28
29
30
31
32
33
34
35
36
37
38
39
40
41
42
43
44
45
46
47
48
49
50
51
52
53
54
55
56
57
58
59
60
61
62
63
64
65

			TDS (mg/L)	EC (mS/m at 25°C)	TDS (mg/L)	EC (mS/m at 25°C)	TDS (mg/L)	EC (mS/m at 25°C)
1	LK01-BT	32	11146	1715	43200	6646	6579	1012
2	LK02-BT	12	1664	256	1743	268	824	127
3	LK03-BT	17	8257	1270	11800	1816	6318	972
4	LK04-BT	8	941	145	2858	440	1251	193
5	LK07-BT	13.5	14212	2187	31620	4865	20610	3171
6	LK08*-BT	4.5	631	97	1315	203	471	73
7	LK09-BT	20.5	893	137	1435	221	694	107
8	LK10-BT	9	496	76	-	-	607	93
9	LK11-BT	13.5	512	79	570	88	303	47
10	LK12-BT	8	544	84	598	92	335	52
11	LK13-BT	23	880	135	1449	223	880	135
12	LK14-BT	16	1049	162	2010	309	1119	172
13	LK15-BT	13	535	82	362	56	132	20
14	LK16-BT	9	377	58	286	44	115	18
15	LK17-BT	21.5	2702	416	5645	869	1564	241
16	LK18-BT	13	579	89	1522	234	1540	237
17	LK19-BT	13.5	1277	197	1522	234	1102	170
18	LK20-BT	9	397	61	1184	183	139	21

Declaration of interests

The authors declare that they have no known competing financial interests or personal relationships that could have appeared to influence the work reported in this paper.

The authors declare the following financial interests/personal relationships which may be considered as potential competing interests:

Cong-Thi Diep, Pham Dieu Linh reports financial support was provided by Ghent University. Cong-Thi Diep, Pham Dieu Linh reports a relationship with Ghent University that includes: funding grants.